Influence of circular RNA topology on microRNA stability

Federico Fuchs Wightman[1, 2*], Jerónimo Lukin[3*], Sebastián Giusti[3], Laureano Bragado[1, 2], Berta Pozzi[4], Paula González[5], Juan P. Fededa[5], Damián Refojo[3#] & Manuel de la Mata[2, 6#]

[1]Universidad de Buenos Aires, Facultad de Ciencias Exactas y Naturales.

[2]CONICET-Universidad de Buenos Aires, Instituto de Fisiología, Biología Molecular y Neurociencias (IFIBYNE), Buenos Aires, Argentina.

[3]Instituto de Investigación en Biomedicina de Buenos Aires (IBioBA) - CONICET - Partner Institute of the Max Planck Society, Godoy Cruz 2390, C1425FQD Buenos Aires, Argentina.

[4]Institute of Cell Biology, University of Bern, Bern, Switzerland.

[5]Instituto de Investigaciones Biotecnológicas "Dr. Rodolfo A. Ugalde", IIB-UNSAM, IIBIO-CONICET, Universidad Nacional de San Martín, Buenos Aires, Argentina.

[6]Universidad de Buenos Aires, Facultad de Ciencias Exactas y Naturales. Departamento de Fisiología, Biología Molecular y Celular.

[*]Contributed equally.

[#]Correspondence: drefojo@ibioba-mpsp-conicet.gov.ar, mmata@fbmc.fcen.uba.ar.

Abstract

Circular RNAs (circRNAs) have been proposed to “sponge” or block microRNAs, a property shared with linear RNAs. Alternatively, certain RNAs induce microRNA destruction through the process of Target RNA-Directed MicroRNA Degradation (TDMD). Whether both linear and circular transcripts are equivalent in driving TDMD is unknown. Here we show that RNA topology is critical for TDMD. Through a novel system that expresses a circRNA while reducing the co-expressed cognate linear RNA, we demonstrate that circRNAs cannot induce TDMD. Interestingly, this is attributed to the circular RNA topology and not to its sequence, which is TDMD-competent in its linear form. Similarly, based on the previous knowledge that CDR1as/ciRS-7 circular RNA protects miR-7 from Cyrano-mediated TDMD, we demonstrate that depletion of CDR1as/CirS-7 reduces mir-7 levels, while overexpression of an artificial

linear version of CDR1as/ciRS-7 drives TDMD. By analyzing RNA sequencing data of a neuron differentiation system, we suggest that circRNA-mediated microRNA stabilization is widespread. Our results support a model in which circRNAs, unlike linear mRNAs, lead to a topology-dependent TDMD evasion, aiding in the stabilization of specific microRNAs.

Keywords: circRNA/microRNA/TDMD

Introduction

Circular RNAs (circRNAs) are long known regulatory RNAs that have gained remarkable attention since the first reports that highlighted their high diversity and abundance (Memczak *et al*, 2013; Hansen *et al*, 2013; Salzman *et al*, 2013; Jeck *et al*, 2013). CircRNAs are covalently closed structures that originate from pre-mRNA backsplicing and therefore lack a poly-A tail and 5'-cap. As a result, given that these terminal modifications are the entry points for the microRNA (miRNA) effector machinery (Bartel, 2018; Jonas & Izaurralde, 2015), circRNAs seem largely immune to miRNA silencing. Furthermore, although current knowledge points towards a diversity of both nuclear and cytoplasmic functions for different individual circRNAs, several findings have suggested that some circRNAs regulate gene expression by working as miRNA "sponges" (Chen, 2020; Xiao *et al*, 2020; Hanan *et al*, 2020).

Whether circRNAs act on miRNAs by blocking them functionally, affecting their stability, or a combination of both remains to be determined. In particular, it is unclear whether circRNAs are active in driving Target Directed MicroRNA Degradation (TDMD), a mechanism that has emerged as central in affecting miRNA turnover. During TDMD, targets with extensive base-pair complementarity towards the 3' end of the miRNA –i.e. displaying no more than 3 mismatches in addition to a central bulge– lead to miRNA degradation, reversing the logic of canonical miRNA target silencing by which the target RNA is conventionally degraded (Ameres *et al*, 2010b; Cazalla *et al*, 2010a; Marcinowski *et al*, 2012; Fuchs Wightman *et al*, 2018). TDMD induces a conformational change on Argonaute (AGO) proteins that leads to their poly-ubiquitination and degradation, rendering the specifically loaded miRNAs unprotected and susceptible to degradation by general nucleases (Shi *et al*, 2020; Han *et al*, 2020). Unlike sponging, TDMD-inducing targets act catalytically even at sub-stoichiometric levels, resulting in the most selective and potent miRNA degradation mechanism described to date and which seems to explain the half-lives

of most naturally unstable miRNAs (de la Mata *et al*, 2015; Denzler *et al*, 2016; Kleaveland *et al*, 2018; Shi *et al*, 2020). A priori, the circular topology of circRNAs should not represent an impediment to regulating miRNAs through TDMD, and circRNAs' high stability could even be an advantage for this activity. Nevertheless, to date no circRNA has been described to drive TDMD and the only available evidence indicates that circRNAs might instead lead to miRNA stabilization (Piwecka *et al*, 2017; Chen *et al*, 2019).

CircRNAs are typically coexpressed with their cognate linear RNAs from the common host genes. However, the circRNA over linear ratio occurs in different proportions, with a subset of circRNAs reaching higher levels than their cognate linear isoforms (Chen, 2020). To reveal insights into circRNA-specific functions and mechanisms, a plethora of publications have relied on circRNA overexpression using various inverted repeat-containing vectors (Memczak *et al*, 2013; Zhang *et al*, 2014; Conn *et al*, 2015; Liang & Wilusz, 2014; Kramer *et al*, 2015; Li *et al*, 2017; Liu *et al*, 2019; Hansen *et al*, 2013; Guarnerio *et al*, 2019; Litke & Jaffrey, 2019). Yet, the capability of plasmid-based methods to overexpress exogenous circRNAs free from overlapping, "leaky" linear RNA expression remains questionable. Thus, attributing any observed effects to the overexpressed circRNA while not rigorously controlling for the potential role of the undesired coexpressed linear transcripts represents a potential pitfall (Pamudurti *et al*, 2017; Kristensen *et al*, 2019; Chen, 2020; Dodbele *et al*, 2021).

A key general question in the field that remains largely unanswered, is whether the circular nature of circRNAs is intrinsically or mechanistically linked to their molecular functions. In this study we aimed to elucidate whether linear and circular target topologies function differently to affect miRNA stability and function. Using a strategy that allows us to express an artificial circRNA with minimal expression of the counterpart linear transcript, we showed that the circular RNA, as opposed to the linear form, is unable to induce TDMD. We also examined the well described CDR1as/ciRS-7-miR-7-Cyrano network of noncoding RNAs, where the lncRNA Cyrano destabilizes miR-7-5p through TDMD (Kleaveland *et al*, 2018), while the circRNA CDR1as/ciRS-7 yields a protection on miR-7-5p (Piwecka *et al*, 2017). We show that expression of an artificially linear version of CDR1as/ciRS-7 triggers TDMD and is unable to rescue the endogenous circRNA loss of function, demonstrating that the circular topology of CDR1as/ciRS-7 is crucial for the evasion of TDMD. Finally, we show that interactions between circRNAs and miRNAs might lead to more general phenomenon of miRNA stabilization, representing a potentially widespread mechanism during neuron-like differentiation.

Results

Artificial circRNA expression

In order to compare the effect of circular and linear RNAs on microRNA stability, we designed constructs capable of expressing high levels of either linear transcripts or artificial circRNAs encompassing segments of identical primary sequence (Figure 1A). Both the linear and circular RNAs contain 4 binding sites for a candidate miRNA (miR-132) with proven TDMD-competent sequence complementarity (de la Mata *et al*, 2015) (Figure S1A). To express the circRNA, we followed a strategy consisting of inserting acceptor and donor splice sites flanking the segment of the transcript to be circularized, plus Alu reverse complementary sequences (RCS) from the introns of a naturally circularized RNA (human ZKSCAN1 exons 2 and 3 respectively), (Figure 1A) (Liang & Wilusz, 2014). In order to preferentially enrich the expression of the circular over the linear variant in neurons, we introduced perfectly matched sites against an endogenous neuronal miRNA (miR-124) which are lost after RNA processing in the backspliced circular product but remain present in the linear RNA isoform, thus rendering the linear –but not the circular– RNA form susceptible to AGO2 slicing (Figure 1A). As a TDMD positive control, we expressed a linear transcript with identical sequence to the artificial circRNA construct, but lacking the splice sites and the reverse complementary flanking introns that induce circularization (Liang & Wilusz, 2014) (Figures 1B and S1A). The latter constructs have been proved effective in triggering TDMD in primary neurons (de la Mata *et al*, 2015). All constructs were packed into lentiviral vectors and used to transduce mouse primary neurons.

To confirm that the expressed circRNA had covalently linked ends and was therefore resistant to RNA exonuclease digestion, we treated total RNA samples with RNase R. We observed that the artificial circRNA was significantly less susceptible to the digestion than the linear transcript, supporting a circular structure (Figure S1B). Next, to rule out artifacts that could be caused by template switching during cDNA synthesis and that could serve as templates for the divergent primers -designed to amplify across the artificial circRNA backspliced junction- (Figure 1A, primer pair 1), we performed the PCR from cDNAs obtained with two different reverse transcriptases (MMLV-RT & Superscript II). Amplification from both cDNAs produced identical PCR products with identical sequences spanning the predicted backsplicing junction (Figure S1C). Because the two RT enzymes are unlikely to jump at the exact same

sequences during a putative template switching event, we conclude the transcripts produced from our expression system are bona fide circRNAs.

In order to validate that our constructs expressed a single circRNA species and no concatemers or other spurious by-products, we performed Northern blot analysis in RNase R treated or untreated samples from HEK293T cells, a cell line where miR-124 is not expressed endogenously. We observed that both artificial circRNA constructs bearing either perfect or seed-mutant sites for miR-124, rendered two bands: an RNase R-resistant circRNA product and an RNase R-sensitive linear RNA form. The linear RNA construct produced a single band (Figure S1D). Importantly, digital quantification of northern blot bands correlated strictly with the RT-qPCR measurements using primers to amplify either the circular isoform exclusively (Figure 1A, primer pair 1) or both the linear and circular isoforms combined – hereafter referred to as Total Output (TO)– (Figure 1A, primer pair 2), further validating the latter method for subsequent analysis (Figure S1E). Finally, to validate that our strategy was successful at expressing a circRNA while selectively degrading its counterpart linear transcript by means of miR-124, a microRNA specifically and highly expressed in neurons, we compared the expression products of the artificial circRNA constructs bearing either perfect or seed-mutant miR-124 binding sites targeting the linear isoform (Figure S1A). To that end we transduced the circRNA artificial constructs into mouse primary neurons and performed RT-qPCR using both the primers described above plus additional primers to amplify the linear isoform exclusively (Figure 1A, primer pair 3). Remarkably, we observed that our strategy led to a potent degradation of "leak" linear RNA without affecting the circRNA levels (Figure 1B). Furthermore, circRNA levels produced from the circRNA-expressing construct were exceedingly higher than from the construct expressing the linear RNA (TDMD positive control), while resulting in equivalent total output levels (Figure 1C). Altogether, these results confirm that our system is effective in expressing circRNAs while reducing the levels of their cognate linear RNAs, making it a generally useful tool in experiments aimed at dissecting circRNA function.

Artificial circRNAs are incapable of triggering TDMD

In order to explore whether linear and circular target topologies function differently to affect miRNA stability through TDMD, we determined the extent to which a circular RNA topology can impact miRNA stability via TDMD in neurons, a cell type known to display a potent TDMD effect (de la Mata *et*

al, 2015). To this end we transduced primary neurons with either linear or circRNA expression constructs bearing TDMD-competent (bulged) or seed-mutant binding sites for miR-132, and measured miR-132 levels by an RT-qPCR Taqman assay. Whereas the linear TDMD inducer was capable of effectively destabilizing miR-132, its circularized version showed no effect on miRNA stability even when both constructs reached similar total RNA levels (Figures 1C and 2A).

In order to determine whether the observed differential effect could be attributed to the inability of the circular RNA to bind to the RISC complex, we set out an RNA immunoprecipitation experiment (RIP) by specifically pulling-down AGO2 and isolating all copurifying RNA species. To this end, we coexpressed FLAG/HA-AGO2 in HEK293T cells together with the different circular RNA constructs followed by immunoprecipitation and RT-qPCR analysis. We observed that the artificial circRNA was effectively pulled down together with AGO2 only when carrying bulged sites for miR-132 but not if the sites were mutated at the miRNA seed-binding region (Figures 2B and S2A-B). These results demonstrate that the circular RNA is indeed able to specifically bind to the RISC complex, ruling out that defects in circRNA-AGO2 binding could account the observed lack of TDMD activity.

In order to exclude the possibility that the observed differences were a trivial consequence of an aberrant localization of the circRNA relative to the linear isoform (Chen, 2020), we performed a purification of nuclear and cytoplasmic subcellular fractions. Our results showed that the artificial circRNA accumulates in the cytoplasm at similar proportions relative to the linear control and is only slightly lower in the nuclear compartment (Figures 2C and S2C-D), suggesting that the inability of the circRNA to trigger TDMD is not related to it being retained in the nucleus.

Circular topology of CDR1as/ciRS-7 is necessary to protect miR-7 from TDMD

To answer whether the inability to trigger TDMD was restricted to our circRNA expression system or if it may actually be observed for other known endogenous circRNAs as well, we studied the case of the CDR1as/ciRS-7-miR-7 interaction (Hansen *et al*, 2011, 2013; Memczak *et al*, 2013). To determine whether the circular topology of CDR1as/ciRS-7 has a role in modulating miR-7 levels, we designed tools to manipulate endogenous CDR1as/ciRS-7 levels in rodent primary neurons (Fellmann *et al*, 2013). In order to knock down CDR1as/ciRS-7 we engineered a lentiviral vector to express a specific shRNAmiR (shCDR1as) and transduced it in primary neurons at high efficiency. Interestingly, the effective

CDR1as/ciRS-7 knockdown achieved did not increase miR-7 levels as expected had CDR1as/ciRS-7 been an active inducer of TDMD on this miRNA. On the contrary, and in line with previous evidence (Piwecka *et al*, 2017), CDR1as/ciRS-7 knockdown reduced miR-7 levels, consistent with a stabilization role of the circRNA on this miRNA (Figure 3A).

To determine whether the observed effect was dependent on CDR1as/ciRS-7's circular topology, we attempted to rescue the CDR1as/ciRS-7 knockdown with the expression of an artificial linear version of CDR1as/ciRS-7 –linCDR1as– lacking the shCDR1as target site. Interestingly, the drop of miR-7 levels caused by the knockdown of the endogenous CDR1as/ciRS-7, could be neither rescued nor enhanced by co-expressing the linear CDR1as/ciRS-7, even though the artificial linCDR1as reached expressions levels similar to those of endogenous CDR1as/ciRS-7 in control cells (Figure 3A). Remarkably, expressing linCDR1as alone –without knocking down endogenous CDR1as/ciRS-7 caused a significant destabilization of miR-7 (Figure 3B), consistent with TDMD being driven by the RNA expressed under an artificial linear RNA topology. Careful inspection of the miR-7 sites present in CDR1as/ciRS-7 showed that no less than 5 of them indeed exhibit a base pairing complementarity compatible with a TDMD-competent architecture (Figure S3A). Importantly, the observed effect on miR-7 caused by overexpression of linear linCDR1as did not correlate with any variation of the endogenous levels of (circular) CDR1as/ciRS-7, arguing against potential indirect effects due to overexpression of the transgene (Figure S3B).

As an orthogonal strategy to reduce CDR1as/ciRS-7 levels and rule out potential off target or indirect effects caused by the shCDR1as, we used CRISPR/Cas9 genome editing to mutate the splicing sites of the endogenous CDR1as/ciRS-7 gene. To that end we expressed two sgRNAs against both donor and acceptor splice sites of CDR1as/ciRS-7 respectively (Figure S3C). Despite an overall lower efficacy in CDR1as/ciRS-7 knockdown reached through CRISPR/Cas9 editing compared to the shCDR1as, we observed a similar effect consistent with CDR1as/ciRS-7 being unable to induce TDMD on miR-7 but rather leading to its stabilization (Figure S3D-E).

To test whether miR-7 destabilization produced by CDR1as/ciRS-7 knockdown also resulted in the expected upregulation of previously described mRNA targets, we measured the levels of four validated miR-7 targets via RT-qPCR. We observed that all four of them were slightly upregulated upon CDR1as/ciRS-7 knockdown relative to control (Figure 3C). Along the same line, reanalysis of RNA

sequencing data from published data further confirmed that miR-7 predicted targets (retrieved from TargetScanMouse v7.1) were significantly upregulated in mouse cortex upon CDR1as/ciRS-7 knockout (Figure 3D-F) (Piwecka *et al*, 2017).

Overall, our results show that endogenous CDR1as/ciRS-7 is unable to trigger TDMD on miR-7 but rather stabilizes this miRNA. Accordingly, only if expressed as an artificially linear RNA can it engage in miR-7 degradation through TDMD, further supporting the notion that the natural circular/linear topology, and not just the linear sequence of a RNA target, is a crucial determinant for engaging in such type of regulation.

CircRNAs potentially stabilize dozens of microRNAs across neuron-like differentiation

Based on our results, we hypothesized that circRNAs might possess the ability to influence miRNA stability through evading TDMD and eventually protecting miRNAs from degradation. Yet, whether this type of regulation could be a widespread phenomenon is unclear. To explore this possibility, we analysed available sequencing data of miRNA, circRNA and mRNA expression from hESC H9 cells both undifferentiated and differentiated into forebrain (FB) neuron progenitor cells (Chen *et al*, 2015; Zhang *et al*, 2016). We reasoned that this model would be appropriate to test our hypothesis from the viewpoint that a significant proportion of circRNAs are regulated along neuron differentiation -with upregulation being more frequent than downregulation (You *et al*, 2015; Rybak-Wolf *et al*, 2015). Concomitantly, neuron-specific miRNAs are known to become more susceptible to degradation in more mature neurons (Krol *et al*, 2010), a scenario where circRNAs could act by selectively regulating miRNA stability. In order to consider only the biochemically supported circRNA-miRNA pairs, we used the CLIP-Seq experimentally supported mRNA-miRNA, lncRNA-miRNA and circRNA-miRNA interaction networks catalogued in the STARBASE v3/ENCORI database (Yang *et al*, 2011; Li *et al*, 2014) as a proxy for bona fide interactions.

We addressed the analysis following two different but complementary approaches. The first one aimed at studying the expression of the most highly "sponged" miRNAs, namely those interacting with multiple and/or highly expressed circRNAs, across differentiation of hESC H9 cells into forebrain neuron progenitor cells. To that end, for every expressed individual miRNA we calculated a "sponging

coefficient". The score was computed by multiplying the number of specific miRNA sites present on each circRNA by the number of backspliced junction reads of each circRNA before differentiation, resulting in the "effective" number of specific miRNA sites contributed by each circRNA. The sum of all effective number of sites contributed by all circRNAs provided a measure of the total effective number of sites for each individual miRNA (Figure 4A, ranked in Supplementary Data 1). The "sponging coefficient" was finally obtained by normalizing this number to each miRNA's expression level before differentiation (Figure 4B, ranked in Supplementary Data 1). According to this analysis, the most highly "sponged" miRNAs, as defined by those with the highest "sponging coefficients", were significantly upregulated across differentiation (Figure 4C). We next sought to determine whether the observed correlation was a consequence of post-transcriptional stabilization of mature miRNAs and not the trivial effect of changes in miRNA gene transcription rates. To that end we estimated the change in pri-miRNA expression levels as a proxy for change in transcription levels of the respective miRNA genes across differentiation. Interestingly, we found that the correlation between fold changes of mature miRNA and pri-miRNA levels was weaker for the most highly "sponged" miRNAs than for the more poorly "sponged" miRNAs, arguing for a stabilization and not a transcriptional effect (Figure 4D). In sum, this analysis is consistent with a miRNA stabilization through the concerted interaction of individual miRNAs with multiple and/or highly expressed circRNAs across differentiation.

As a complementary approach, we aimed at analysing the expression of the potentially most highly "sponging" circRNAs, namely those potentially interacting with multiple miRNAs across differentiation into forebrain neuron progenitor cells. To that end we calculated the total number of sites (for all miRNAs) present on each circRNA, which resulted in the total number of predicted "effective" sites (Figure 4E and Supplementary Data 1). Interestingly, we observed that an increasing number of effective sites present on circRNAs does not correlate with an obvious decrease in circRNA fold change expression across differentiation, which is consistent with the notion that circRNAs are immune to miRNA regulation (Figure 4F). The collection of miRNAs and circRNAs interacting across this neuron-like differentiation might include more than a hundred miRNAs and dozens of circRNAs. In fact, by focusing on the predicted most highly sponging circRNAs, this analysis further illustrates that circRNAs with the highest "sponging" capacity for miRNAs lie at highly connected nodes within a

complex regulation network, further supporting the view that individual circRNAs might act as potential scaffolds for multiple miRNAs (Figure S4A).

Discussion

A long-lasting and largely unresolved question in the field is whether circRNAs' topology, i.e. their circular nature, is intrinsically relevant for them to exert their molecular actions. Alternatively, the circular form of some circRNAs might have been evolutionarily selected merely based on their resistance to endonucleases that confer them special stability properties. Due to different technical reasons, many of which are related to the expression systems employed, these key questions have not been fully addressed so far.

While most experimental approaches have largely relied on knocking down or overexpressing circRNAs in different organisms or cultured cells, undesirable artifacts can very commonly act as confounding factors in the interpretation of the results. In particular, overexpression of circRNAs suffers from a major caveat related to the unwanted linear RNA species that are inevitably co-expressed from the commonly used expression vectors. This type of problem can easily lead to conclusions where functions are wrongly assigned to circRNAs under circumstances where the associated linear transcripts are the true functional molecules but are ignored in the experiments (Dodbele *et al*, 2021). We have addressed this issue by designing a strategy that allows us to express circRNAs while keeping expression of the counterpart linear product to a minimum. A similar strategy was previously reported in a different context with the goal of restricting expression of transgenes to specific tissues (Brown *et al*, 2007). In our hands the approach proved to work as an efficient tool to deliver high levels of circRNAs while limiting the expression of the linear RNA derived from the circRNA construct (Figure 1).

We have exploited this tool to gain insight into the mechanism of the well-known role of circRNAs in blocking miRNAs. Despite being neither prevalent nor unique to circRNAs as a class, the capacity to inhibit or "sponge" miRNA silencing activity has been the most extensively documented function of circRNAs (Chen, 2020; Dodbele *et al*, 2021). This abundance of papers likely obeys to historical reasons, namely the fact that this was the first function to be reported for circRNAs since their rediscovery during the last decade (Memczak *et al*, 2013; Hansen *et al*, 2013). In spite of this, a clear picture of the mechanism by which some circRNAs act on miRNAs is still missing. For instance, it remains

unclear whether circRNAs act on microRNAs simply by blocking their function and/or by affecting their stability. In this sense, although it has been speculated that circRNAs might trigger TDMD like linear RNAs, this premise was never formally and experimentally tested so far (Gasparini *et al*, 2020). Our data suggest the opposite: even when expressed at comparable levels, artificial circular RNAs of identical sequence to those of TDMD-inducing linear RNAs, prove incapable of inducing TDMD (Figure 2). This is largely recapitulated by the endogenous circRNA CDR1as/ciRS-7 which cannot trigger TDMD on miR-7 –in fact it leads to its stabilization as discussed below– unless artificially expressed as a linear RNA.

The fact that the protection of miR-7 exerted by CDR1as/ciRS-7 was not recapitulated by our artificial circRNA on miR-132, might be explained by the emergent properties of the CDR1as/ciRS-7-miR-7-Cyrano network. Based on this idea, the stabilization of miR-7 might emerge from the inability of CDR1as/ciRS-7 to drive TDMD in combination with its preserved ability to bind and compete for miR-7, ultimately shielding the exceptionally potent TDMD activity driven by Cyrano on miR-7 (Kleaveland *et al*, 2018). A similar reasoning might apply to the fact that the artificial (linear) linCDR1as, when expressed in combination with the knockdown of endogenous (circular) CDR1as/ciRS-7, does not produce any additional reduction of miR-7 levels: under these conditions, an unleashed Cyrano-driven TDMD activity acting on miR-7 might reach a limit in miR-7 degradation rate which cannot be further enhanced by an additional TDMD-competent target such as linCDR1as. In the presence of CDR1as/ciRS-7, the system would be set to intermediate miR-7 degradation rates which could be further enhanced by other TDMD-competent RNAs such as linCDR1as (see model in Figure S4B). Notably, a similar protection phenomenon has been observed in a prostate cancer cell line, where knockdown of circCSNK1G3 bearing binding sites for miR-181b/d decreased their abundance, while circCSNK1G3 overexpression increased it (Chen *et al*, 2019).

The molecular basis explaining the functional differences between circRNAs and their cognate linear transcripts in triggering TDMD, might obey to the structural properties affected by the circular-linear topology. Based on a previous report, whereas circRNAs inhibit PKR-mediated innate immune responses, their cognate linear counterpart transcripts cannot. The explanation behind this phenomenon seems to be the inherent ability of circRNAs to fold into more stable short local secondary structures compared to their linear counterpart transcripts. This in turn seems to lead to a more stable interaction between circRNAs and PKR (Liu *et al*, 2019). Based on similar principles –but with an opposite

outcome– the greater tendency of circRNAs to form secondary structures could confer them an extra rigidity that could ultimately limit their capacity to drive TDMD. This seems in agreement with previous reports showing that an extended miRNA:target basepairing *per se* is not enough to trigger TDMD: miRNA binding must also occur within a conformationally flexible region of the target for TDMD to be active (Pawlica *et al*, 2016; Fuchs Wightman *et al*, 2018; Li *et al*, 2021). In line with this idea, two in-depth studies have contributed to our understanding of TDMD by pinpointing the ubiquitin ligase ZSWIM8 as a mediator of the mechanism (Shi *et al*, 2020; Han *et al*, 2020). These findings showed that the binding of TDMD-competent target RNAs drives a conformation change on AGO proteins (loaded with specific miRNAs) that leads to their poly-ubiquitination and degradation, leaving the specific miRNAs unprotected and susceptible to degradation by general nucleases. The extra rigidity of circRNAs could preclude the conformational change of AGO, thus bypassing TDMD while remaining bound to the RISC complex. A recent report might be consistent with this view by showing differences between the thermodynamic properties of linear and circular RNA in binding to complementary short RNAs, favouring a model where circRNAs might bind to miRNAs more efficiently than their cognate linear RNAs (Petkovic *et al*, 2021).

An alternative explanation could relate to the differential ability of distinct RNA species in recruiting TDMD machinery factors such as ZSWIM8. In that sense, several characteristics of circRNAs could be critical such as their lack of capping and poly-A tails, although the latter seems dispensable for TDMD based on the fact that HSUR-1, which lacks a poly-A tail, effectively drives TDMD on miR-27 (Cazalla *et al*, 2010b; Pawlica *et al*, 2016). Additionally, specific sequence elements within linear transcripts are required for TDMD. For instance, both the miR-7 and miR-17 binding sites that exist within known TDMD-inducing targets (Cyrano and HCMV's UL144-145 respectively), depend on sequences that are located outside of the miRNA site *per se* for efficiently triggering of TDMD (Lee *et al*, 2013; Han *et al*, 2020; Kleaveland *et al*, 2018). Such sequences might be absent or simply occluded within the more highly structured circRNAs, possibly explaining their observed inability to drive TDMD.

An increasing number of TDMD natural examples have arisen in the past few years, including both endogenous targets capable of destabilizing specific miRNAs and viral transcripts which in doing so facilitate infection (Ameres *et al*, 2010a; Cazalla *et al*, 2010b; Li *et al*, 2017; Bitetti *et al*, 2018; Ghini *et al*, 2018; Li *et al*, 2021; Simeone *et al*, 2022). Furthermore, the discovery that TDMD is more widespread

than initially thought suggests that many more instances of endogenous TDMD will be discovered (Shi *et al*, 2020; Han *et al*, 2020). In this scenario, circRNAs' capacity to evade such regulation could confer them an advantage in regulating miRNA stability even when involving highly complementary pairing architectures that would otherwise drive TDMD in the context of linear RNAs. As a result, circRNAs may achieve an indirect stabilization of miRNAs by specifically sequestering and rendering them unavailable for TDMD. This type of regulation would in turn be compatible with a potential reversibility of circRNA's inhibitory function on miRNAs.

Interactions between miRNAs and competing-endogenous RNAs (ceRNAs) have received a broad attention in the recent years as they might represent a mechanism of miRNA inhibition (Tay *et al*, 2014). However, due to stoichiometry considerations, the likelihood that individual ceRNAs titrate the total amount of miRNA available for target repression seems limited (Denzler *et al*, 2014, 2016; Jens & Rajewsky, 2015; Bosson *et al*, 2014; Pinzon *et al*, 2017). Instead, models where multiple ceRNAs regulate single miRNAs have been favoured (Ameres & Zamore, 2013; Dodbele *et al*, 2021). The case of CDR1as/ciRS-7-miR-7 pair might represent an outstanding example functioning in an analogous way: CDR1as/ciRS-7 is a highly expressed circRNA with > 60 evolutionarily conserved miR-7 binding sites based on previous reports (Memczak *et al*, 2013; Hansen *et al*, 2013) (67 predicted sites for miR-7 in humans based on the STARBASE/ENCORI database), significantly exceeding the average number of sites annotated for circRNAs (based on Starbase/ENCORI database, see Supplementary Data 2). On the other hand, while CDR1as/ciRS-7 is highly expressed in human, rat and mouse brain, miR-7 tends to display medium to low expression. Our results favour a model where the concerted interaction of multiple circRNAs with individual miRNAs seems the most likely and relevant scenario in regulating miRNA stability. Interestingly, among the miRNAs that are upregulated upon ZSWIM8 knockdown in mouse induced neurons (Shi *et al*, 2020), two belong to the most "sponged" miRNAs according to our analysis (miR-7 and also miR-409-3p), suggesting that such type of regulation might be acting in neuron differentiation and possibly in pathophysiological conditions.

A complex and yet unresolved aspect of the role of circRNAs in regulating miRNAs relates to our inability to predict their outcome on canonical miRNA silencing activity. In this sense, depending on the relative binding site architectures and the relative stoichiometries of the molecules involved, different outcomes may be expected. For instance, miRNA stabilization could lead to greater average target

repression due to an increased abundance of the miRNA. This is indeed observed for miR-7 targets in primary neurons upon CDR1as/ciRS-7 KD (Figures 3F-H) (Piwecka *et al*, 2017). However, miRNA stabilization may also be accompanied by an overall tight blockade of miRNA silencing activity, leading to opposite outcomes in different contexts. Such could be the case of miR-181b/d in a prostate cancer model, where its decreased abundance upon circCSNK1G3 knockdown (resembling the case of miR-7 and CDR1as/ciRS-7), leads to downregulation of miR-181b/d predicted targets (Chen *et al*, 2019) (Figures S3G and H). Eventually, more in-depth knowledge of the players involved, their dynamics and relative stoichiometries will help us understand the emergent properties arising from different systems and the full potential and adaptive value of circRNAs in miRNA regulation.

Materials and methods

Plasmid construction

Unless otherwise specified, the lentiviral vectors are based on pRRLSIN.cPPT.SYN.WPRE (de la Mata *et al*, 2015).

Linear CDR1as/ciRS-7 was amplified by PCR from rat genomic DNA (see primers at Supplementary Table 1). Following gel purification (QIAquick Gel Extraction Kit), and cloning into pCR II-Blunt-TOPO (ThermoFisher) it was then subcloned into pRRLSIN.cPPT.SYN.WPRE. The linear CDR1as/ciRS-7 version lacking the shCDR1as target site -linCDR1as^{671}- was done by PCR amplification and re-cloning in the original backbone (Supplementary Table 1), eliminating the BamHI-SalI segment containing the full linCDR1as. The linear transcript used as a negative control consists of mCherry carrying four mutated sites for miR-7, obtained by eliminating the miR-132 sites (NheI-SalI) from an already published linear TDMD inducer (de la Mata *et al*, 2015) and adding miR-7 sites by Gibson Assembly (Gibson *et al*, 2009) and a gBlock (Integrated DNA Technologies, see sequence at Supplementary Table 1).

The pri-miR-132 and pri-miR-124 expressing constructs were made by eliminating the BamHI-BsrGI portion of pRRLSIN.cPPT.SYN.WPRE and amplifying the pri-miRs (Supplementary Table 1) from miRNASelectTM pEGP-mmu-mirna expression vectors (Cell Biolabs).

The shRNAmiR (shCDR1as) is an engineered version miR-671 -previously described as a natural CDR1as/ciRS-7 regulator (Piwecka *et al*, 2017; Kleaveland *et al*, 2018)- designed to be fully complementary to the circRNA and maximizing its slicing (Figure 3A). The shCDR1as lentiviral vector

was constructed by removing the pri-miR from one of the previously made vectors using BamHI-NheI (Supplementary Table 1), and inserting a synthetic DNA (gBlock gene fragment, IDT) by Gibson Assembly (Gibson *et al*, 2009).

Plasmid for artificial circRNA expression was constructed using the same procedure, using gBlocks (Integrated DNA Technologies) with the ZKSCAN1 upstream and downstream introns (Liang & Wilusz, 2014) flanking mCherry and miR-132 sites (de la Mata *et al*, 2015). We later added the sites for miR-124 by exchanging mCherry from a linear TDMD inducer, XhoI, for the circularizing portion XhoI-SalI. Finally, we swapped the SYN promoter, XbaI-BamHI, for TREp (see Figure 1A and Supplementary Table 1). As a positive control for degrading miR-132, we used a previously described linear TDMD inducer consisting of mCherry with miR-132 sites (de la Mata *et al*, 2015). The tetracycline-inducible promoter (TREp) was amplified from the plasmid SYN-Tetoff-GFP (Gascón *et al*, 2008). Three different variants of the artificial circRNA were made: one with 4x TDMD-inducing (bulged) miR-132 sites in the circularizing segment and 4x perfectly matched sites for miR-124 only present in the linear isoform; the other two variants have either miR-132 or miR-124 mutated sites.

The lentiviral vector driving expression of FLAG/HA-AGO2 (human) from the Syn promoter (pLV-FLAG-HA_AGO2) was generated by amplifying FLAG/HA-AGO2 from pIRESneo-FLAG/HA AGO2 (Addgene plasmid 10822).

The construct for CRISPR/Cas9 genome editing of CDR1as/ciRS-7 splicing sites is based on lentiCRISPR v2 (Addgene plasmid 52961), following the Zhang Lab protocol (Sanjana *et al*, 2014; Shalem *et al*, 2014). See primers at Supplementary Table 1.

HEK293T culture and transient transfection

HEK293T cells were available in our institute. Cells were tested for mycoplasma contamination and only clean stocks were further used for our experiments. Cells were grown in DMEM-F12 (Gibco) supplemented with 10% (v/v) FCS and 25 U/mL Penicillin-Streptomycin (Gibco) and were plated for transfection at 100,000 cells/well on 24-well plates. One day after plating, cells were transfected using the PEI method with the following plasmids: the artificial circRNA expressing construct, the linear TDMD inducers and/or the FLAG/HA-AGO2 plasmid. Co-transfected were the pri-miR-132, pri-miR-124 and/or

433 tTA expressing vectors when appropriate. The optimal amount of pri-miR-132 transfected had been
434 previously described (de la Mata *et al*, 2015).
435

436 ## Lentivirus production and transduction

437 Recombinant lentiviral particles were produced in HEK293T cell line. Cells were co-transfected using the
438 PEI method with the lentiviral expression vector and two packaging vectors: pMD2.G (Addgene plasmid
439 12259), a plasmid expressing the VSV-G envelope gene, and pCMVR8.74 (Addgene plasmid 22036), a
440 plasmid expressing the gag/pol genes (2nd generation lentiviral packaging plasmid). The supernatants
441 containing the viral particles were collected 48–72 h after transfection and concentrated using
442 centrifugal filter units (Amicon Ultra-15, molecular weight cutoff 100 kDa, Millipore Cat. # UFC910024).
443 Viral titers were determined semi-quantitatively by serial dilution on primary hippocampal neurons and
444 observation of GFP/mCherry infected cells. In turn, MOIs correlated well with the measured GFP mRNAs,
445 allowing us to achieve similar expression levels across several experiments by infecting at similar MOIs.
446

447 ## Animals used in this study

448 All animal tissues used in this study were obtained under experiment protocol no. No.2020-04-DR with
449 the approval from the Comisión Institucional para el Cuidado y Uso de los Animales de Laboratorio
450 (CICUAL) at the Instituto de Investigación en Biomedicina de Buenos Aires (IBioBA) – CONICET – Partner
451 Institute of the Max Planck Society.
452

453 ## Neuronal cultures and lentiviral transduction

454 Cortical and hippocampal neurons were dissected from embryonic day 16.5 and 18.5 (E16.5 and
455 E18.5) respectively CD1 embryos of mixed sex. Culture preparation was performed as previously
456 described (Giusti *et al*, 2014; Vogl *et al*, 2015). Briefly, cortex from CD1 mouse embryos were dissected
457 and a neuronal suspension was prepared through Trypsin digestion and mechanical disruption of the
458 tissue. Neurons were plated in 24 multi-well plates at a density of 80cells/mm2 (150.000 cells per well)
459 and maintained in Neurobasal-A media (ThermoFisher) with 2% B27 and 0.5 mMGlutaMAX-I
460 (ThermoFisher) at 37 °C and 5% CO2. CD1 mice for neuronal cultures were provided by our Specific
461 Pathogen Free Animal Facility.

462 The euthanasia of the animals to generate primary neuronal cultures was performed under
463 experiment protocol no. 2020-04-DR which was evaluated by the Institutional Animal Care and Use
464 Committee of the IBioBA-CONICET according to the Principles for Biomedical Research involving
465 animals of the Council for International Organizations for Medical Sciences and provisions stated in the
466 Guide for the Care and Use of Laboratory Animals.

467 Neurons were transduced 4-7 days after plating (DIV4-7) with either of the following lentiviral
468 constructs: linCDR1as, linCDR1as$^{671\text{-}}$, shCDR1as, the linear control or a combination of these,
469 appropriately described in Results and Figures. The vectors driving each of the artificial circRNAs
470 expressions were transduced in combination with a lentiviral construct expressing the tetracycline-
471 controlled transactivator protein (LV-Syn-tTA). RNA was extracted at DIV11 as indicated below.

472

473 FLAG/HA-AGO2 transfection and immunoprecipitation (AGO2 RIP)

474 The FLAG/HA-AGO2 expressing plasmid was transfected into HEK293T cells as described above.
475 Immunoprecipitation of FLAG/HA-AGO2 was performed with Anti-FLAG M2 Magnetic Beads (Sigma.
476 Cat # M8823). Beads were washed twice with TBS buffer (50 mM Tris HCl, 150 mM NaCl, pH 7.4). For each
477 immunoprecipitation (IP), one 6-cm plate with 50% confluency was used. Cells were washed once with
478 cold PBS and lyzed in 500 µl of lysis buffer [50 mM Tris–HCl pH 7.5, 150mM NaCl, 1% (v/v) TRITON X-100,
479 1 mM EDTA, containing protease inhibitors (cOmplete, EDTA-free Protease Inhibitor Cocktail, Roche)
480 and RNase inhibitor (Invitrogen)]. The lysates were incubated 30 minutes on ice, cleared by
481 centrifugation at 16,000 g for 10 minutes at 4 degrees and mixed with the washed beads. After 2 hours
482 of rotation at 4 degrees, the beads were washed three times with TBS buffer. As a control for the IPs,
483 non-transfected HEK293T cells were used. FLAG/HA-AGO2 expression and immunoprecipitation
484 efficiency were determined by Western blot using anti-HA antibody (clone 3F10, Roche). Monoclonal
485 antibody against Actin was purchased from Chemicon (MAB1501). Antibodies against α-Tubulin and
486 Histone-3 were purchased from Santa Cruz Biotechnology. RNA was extracted by adding Trizol reagent
487 (Invitrogen) directly on the beads.

488

489 Subcellular fractionation

Briefly, the artificial circRNA expressing construct and the linear control were transfected into HEK293T cells as described above, in 6-well plates at 50% confluency. After 48 hours, cells were harvested using 500 μl of PBS, transferred to a microcentrifuge tube and centrifuged at 500 g for 5 minutes. The supernatant was discarded, and the pellet resuspended in 350 μl of PBS plus 0.1% NP-40 (IGEPAL). 150 μl were separated and called TOTAL fraction. The remaining volume was centrifuged for 10 seconds at 10,000 rpm. 150 μl of the supernatant were separated and called CYTOPLASM fraction. The pellet was resuspended in 150 μl of PBS plus 0.1% NP-40 (IGEPAL) and centrifuged again at 10,000 rpm. The supernatant was discarded, and the pellet resuspended in 150 μl of PBS plus 0.1% NP-40 (IGEPAL). This was called the NUCLEAR fraction.

Out of the 150 μl of each fraction, 75 μl were used for Western Blotting and 75 μl for RNA extraction followed by reverse transcription and quantitative polymerase chain reaction (RT-qPCR).

RNA extraction

Total RNA extractions were made using Trizol reagent (Invitrogen) following the manufacturer's instructions.

RT-qPCR quantification

MiRNA and U6 levels were determined by using Taqman® microRNA Assays (Applied Biosystems) following the manufacturer's instructions. MicroRNA levels were normalized to U6 RNA levels. Standard curves for the analyzed miRNAs and U6 RNA were performed with serial dilutions of selected cDNAs, allowing calculation of relative levels. For quantification of target mRNAs, the different isoforms of the artificial circRNA constructs and CDR1as/ciRS-7, total RNA was treated with RNase-free DNase I (DNA-freeTM Kit, Ambion) and reverse transcribed using random hexamers and SuperScriptTM II Reverse Transcriptase (Invitrogen), following the manufacturer's instructions. Target mRNA, the different isoforms of the artificial circRNA constructs levels and CDR1as/ciRS-7 were determined by SYBR green qPCR using a custom-made qPCR mix (Supplementary Table 2) and specific primers (detailed at Supplementary Table 3). Alternatively, INBIO highway qPCR SYBR green mix was used (Ref M130). Standard curves for the analyzed amplicons were done with serial dilutions of selected cDNAs, allowing calculation of relative levels.

Northern blot analysis

Northern blot analysis was performed according to standard procedures (Roditi *et al*, 1987). A total amount of 10 μg of RNA was loaded in each lane. The radioactively labelled probe, corresponding to the mCherry CDS fragment, was prepared using the Megaprime DNA labelling kit (Amersham Biosciences) according to manufacturer's instructions. The 18S RNA from the agarose gel run was used as loading control. Blots were hybridized at 65° and washed in 0.2× SSC/0.1% SDS. The blots were exposed to Phosphorimager screens and scanned with Typhoon FLA 7000 (GE Healthcare Life Sciences). The relative intensities of the bands were measured by densitometry using ImageJ.

Western blot analysis

Protein samples were separated on 12% SDS-polyacrylamide gels and transferred to PVDF membranes. Membranes were incubated with primary antibodies: anti-HA 3F10 (Rat, 1:2500), anti-Tubulin (polyclonal rabbit anti βtubulin H-235 from Santa Cruz Biotechnology, 1:2500) and Histone-3 (polyclonal rabbit anti H3 H-0164 from Merk, 1:2500). After washing, membranes were incubated with IRDye® 800CW (LI- COR Biosciences) secondary antibodies. Bound antibody was detected an Odyssey imaging system (LI-COR Biosciences).

Statistical analysis

All key experiments of this study were repeated at least three times, producing biological sample sizes (n) ≥3. R programming language was used to process information, visualize and design graphs, and perform statistical tests. Data was normalized and scaled across experiments using Unit Length Normalization. Briefly: transform x to x' by dividing each value of the feature vector by the Euclidean length of the vector. Bar, line, scatter and boxplots were designed using the ggplot2 (Wickham, 2016) and ggpubr packages. Statistical tests were done using base R, ggsignif (https://www.rdocumentation.org/packages/ggsignif/versions/0.6.1) and/or ggpubr (https://rpkgs.datanovia.com/ggpubr/index.html). For those experiments where two conditions were compared, we performed one-sided t-tests, and for those with three conditions, two-sided t-tests (ns: p > 0.05, *: p <= 0.05, **: p <= 0.01, ***: p <= 0.001, ****: p <= 0.0001). When comparing several miR-7

548 targets across conditions, we did a two-way ANOVA followed by Tukey multiple comparisons, showing
549 the adjusted p-values. Error bars represent the standard deviation of the mean (SEM).
550

551 **Bioinformatic analysis of circRNA-miRNA interactions**

552 Two publicly available datasets produced by the Chen Lab were combined to generate a
553 comprehensive analysis taking into account miRNA, circRNA and mRNA expression during
554 differentiation of H9 (hESC) cells to H9 forebrain neurons. From GEO Accession GSE73325 (Zhang *et al*,
555 2016) we obtained data for circRNA and mRNA expression. From GEO Accessions GSE56152 and
556 GSE63709 (Chen *et al*, 2015) we obtained data for microRNA expression. Noteworthy, although the
557 same procedure for differentiation was followed (Zhang *et al*, 2016; Chen *et al*, 2015), sequencing was
558 done on different days (D26 and D35, respectively). We realize this is suboptimal, nevertheless we
559 decided to proceed with the analysis since its goal was limited to the finding of potential candidates
560 that might be suffering from a similar type of regulation as CDR1as/ciRS-7-miR-7.
561 Data of the interaction between circRNAs and miRNAs was retrieved from Starbase/ENCORI v3 database
562 (http://starbase.sysu.edu.cn; (Yang *et al*, 2011; Li *et al*, 2014)). This particular source was selected
563 because it combines site prediction by several programs with experimental validation (e.g., by CLIP).
564 The main parameters chosen for downloading through their API were: assembly = hg19, geneType=
565 circRNA & miRNA, clipExpNum=1, program= all, programNum= 2, target= all and cellType= all.
566 A condensed spreadsheet summarizing all the previously mentioned data can be found at
567 Supplementary Data 3.
568 The analysis was done in R, briefly:

569 • The expression tables were loaded and merged using the Tidyverse package (Wickham *et al*,
570 2019), while the circRNA-miRNA interactions table was joined using the Fuzzyjoin package
571 (https://CRAN.R-project.org/package=fuzzyjoin) to consider genomic locations of both the
572 circRNAs and the miRNA sites.
573 • Log_2 fold changes were calculated for each type of RNA.
574 • The total amount of validated sites each miRNA has on each circRNA (when present) was
575 added.

- A relative number of available sites per circRNA for each miRNA was determined by multiplying the number of sites the miRNA has on a given circRNA by that circRNA's junction reads.
- By adding all the sites miRNAs have among circRNA (and their expression), a total amount of available sites was calculated (referred to as 'effective' sites later on).
- A "sponging coefficient" was defined by taking the total amount of available sites of a certain miRNA and dividing it for its expression (pre-differentiation).
- Two different sets of candidates were highlighted using different criteria:
    - Most "sponged" microRNAs, according to the "sponging coefficient".
    - Most "sponging" circRNAs, considering the number of sites each circRNA carries for all miRNAs multiplied by the number of junction reads.
- All graphs were programmed and illustrated using ggplot2 package (Wickham, 2016), ggrepel package (https://CRAN.R-project.org/package=ggrepel), hrbrthemes package (https://CRAN.R-project.org/package=hrbrthemes) and/or viridis package (https://CRAN.R-project.org/package=viridis), except for the network diagram (Figure S4A) which was done using IGraph package (https://igraph.org/r/). Statistical analysis of the boxplots was done and added to the graphs using ggsignif (https://www.rdocumentation.org/packages/ggsignif/versions/0.6.1) and/or ggpubr (https://rpkgs.datanovia.com/ggpubr/index.html).
- For pri-miRNA analysis we used the Galaxy platform (Afgan *et al*, 2018). Briefly, raw reads were trimmed using Trim Galore! and mapped to the human reference genome (hg38) with the RNA-STAR aligner (Dobin *et al*, 2013). Pri-miR counts were obtained from the mapped BAM files using featureCounts (Liao *et al*, 2014) and the annotation file (has.gff3) retrieved from miRBase (Kozomara *et al*, 2019).

Bioinformatic analysis of miR-7 and miR-181b/d targets

Targets for miR-7 were retrieved from TargetScan 7.1 mouse (Agarwal *et al*, 2015) while the ones for miR-181b/d from TargetScan 7.2 human (Agarwal *et al*, 2015). Raw RNA-seq counts were downloaded for CDR1as/ciRS-7 KO data (Piwecka *et al*, 2017) and circCSNK1G3 KD (Chen *et al*, 2019), accessions GSE93130 and GSE113124, respectively. A differential expression analysis was done using the DESeq2

605 package (Love *et al*, 2014). Graphs were made using the results of the analysis and the packages
606 mentioned above.
607

608 Acknowledgements

609 We thank Isabel Roditi for providing materials and discussing experiments, Helge Grosshans and
610 Alberto R. Kornblihtt for a critical reading of the manuscript. M.d.l.M. is funded by grants from Agencia
611 Nacional de Promocion Cientifica y Tecnológica (ANPCyT) of Argentina (PICT- 2016-0499 and PICT-2018-
612 0478_PRH 2016-0002). D.R. acknowledges the support of the Volkswagen, Stiftung, the Max Planck
613 Society, the Fondo para la Convergencia Estructural de Mercosur (COF 03/11), the Agencia Nacional de
614 Promoción Científica y Tecnológica (ANPCyT) of Argentina (PICT- 2019-0499 and PICT-PRH 2014-3782)
615 and the Ministerio de Ciencia, Tecnología e Innovación Productiva of Argentina (MinCyT-BMBF
616 AL15/10). J.P.F. is funded by grants from Ministerio de Ciencia, Tecnología e Innovación Productiva of
617 Argentina (MINCyT) (BMBF/MINCYT MIGRAMIRNA Al/17/05), Agencia Nacional de Promocion Cientifica
618 y Tecnologica (ANPCyT) of Argentina (PICT-2017-2401, PCE-GSK-2017-0052), Glaxo-SmithKline (PCE-
619 GSK-2017-0052) and Fundación Progreso de la Medicina (GF N03/2017).
620

621 Author contributions

622 D.R. and M.d.l.M. conceived the project and designed and interpreted the experiments. F.F.W. and J.L.
623 designed, performed and interpreted most of the experiments. F.F.W. conceived, performed and
624 interpreted all bioinformatics analysis. J.L. and S.G. handled animals and prepared the neuron primary
625 cultures. L.B. performed the subcellular fractionation experiments. B.P. performed the northern blot
626 analysis. P.G. performed the subcloning of some of the constructs used in the study. J.P.F. designed
627 some of the experiments and discussed experimental strategies. D.R. and M.d.l.M. co-supervised the
628 whole project. The manuscript was written by F.F.W., D.R. and M.d.l.M.
629

630 Conflict of interest

631 The authors declare that they have no conflict of interest.

References

Afgan E, Baker D, Batut B, van den Beek M, Bouvier D, Čech M, Chilton J, Clements D, Coraor N, Grüning BA, *et al* (2018) The Galaxy platform for accessible, reproducible and collaborative biomedical analyses: 2018 update. *Nucleic Acids Res* 46: W537–W544

Agarwal V, Bell GW, Nam JW & Bartel DP (2015) Predicting effective microRNA target sites in mammalian mRNAs. *Elife* 4: 1–38

Ameres SL, Horwich MD, Hung J-H, Xu J, Ghildiyal M, Weng Z & Zamore PD (2010a) Target RNA-directed trimming and tailing of small silencing RNAs. *Science* 328: 1534–9

Ameres SL, Horwich MD, Hung JH, Xu J, Ghildiyal M, Weng Z & Zamore PD (2010b) Target RNA-directed trimming and tailing of small silencing RNAs. *Science (80-)* 328: 1534–1539

Ameres SL & Zamore PD (2013) Diversifying microRNA sequence and function. *Nat Rev Mol Cell Biol* 14: 475–488 doi:10.1038/nrm3611 [PREPRINT]

Bartel DP (2018) Metazoan MicroRNAs. *Cell* 173: 20–51

Bitetti A, Mallory AC, Golini E, Carrieri C, Carreño Gutiérrez H, Perlas E, Pérez-Rico YA, Tocchini-Valentini GP, Enright AJ, Norton WHJ, *et al* (2018) MicroRNA degradation by a conserved target RNA regulates animal behavior. *Nat Struct Mol Biol* 25: 244–251

Bosson AD, Zamudio JR & Sharp PA (2014) Endogenous miRNA and target concentrations determine susceptibility to potential ceRNA competition. *Mol Cell* 56: 347–359

Brown BD, Gentner B, Cantore A, Colleoni S, Amendola M, Zingale A, Baccarini A, Lazzari G, Galli C & Naldini L (2007) Endogenous microRNA can be broadly exploited to regulate transgene expression according to tissue, lineage and differentiation state. *Nat Biotechnol* 25: 1457–1467

Cazalla D, Yario T, Steitz J a & Steitz J (2010a) Down-regulation of a host microRNA by a Herpesvirus saimiri noncoding RNA. *Science* 328: 1563–6

Cazalla D, Yario T & Steitz JA (2010b) Down-regulation of a host microRNA by a Herpesvirus saimiri noncoding RNA. *Science (80-)* 328: 1563–1566

Chen L (2020) The expanding regulatory mechanisms and cellular functions of circular RNAs. *Nat Rev Mol Cell Biol* 21: 475–490

Chen S, Huang V, Xu X, Livingstone J, Soares F, Jeon J, Zeng Y, Hua JT, Petricca J, Guo H, *et al* (2019) Widespread and Functional RNA Circularization in Localized Prostate Cancer. *Cell* 176: 831-

843.e22

Chen T, Xiang JF, Zhu S, Chen S, Yin QF, Zhang XO, Zhang J, Feng H, Dong R, Li XJ, *et al* (2015) ADAR1 is required for differentiation and neural induction by regulating microRNA processing in a catalytically independent manner. *Cell Res* 25: 459–476

Conn SJ, Pillman KA, Toubia J, Conn VM, Salmanidis M, Phillips CA, Roslan S, Schreiber AW, Gregory PA & Goodall GJ (2015) The RNA binding protein quaking regulates formation of circRNAs. *Cell* 160: 1125–1134

de la Mata M, Gaidatzis D, Vitanescu M, Stadler MB, Wentzel C, Scheiffele P, Filipowicz W & Großhans H (2015) Potent degradation of neuronal miRNAs induced by highly complementary targets. *EMBO Rep* 16: 500–511

Denzler R, Agarwal V, Stefano J, Bartel DP & Stoffel M (2014) Assessing the ceRNA Hypothesis with Quantitative Measurements of miRNA and Target Abundance. *Mol Cell* 54: 766–776

Denzler R, McGeary SE, Title AC, Agarwal V, Bartel DP & Stoffel M (2016) Impact of MicroRNA Levels, Target-Site Complementarity, and Cooperativity on Competing Endogenous RNA-Regulated Gene Expression. *Mol Cell* 64: 565–579

Dobin A, Davis CA, Schlesinger F, Drenkow J, Zaleski C, Jha S, Batut P, Chaisson M & Gingeras TR (2013) STAR: ultrafast universal RNA-seq aligner. *Bioinformatics* 29: 15–21

Dodbele S, Mutlu N & Wilusz JE (2021) Best practices to ensure robust investigation of circular RNAs: pitfalls and tips. *EMBO Rep* 22: 1–12

Fellmann C, Hoffmann T, Sridhar V, Hopfgartner B, Muhar M, Roth M, Lai DY, Barbosa IAM, Kwon JS, Guan Y, *et al* (2013) An optimized microRNA backbone for effective single-copy RNAi. *Cell Rep*

Fuchs Wightman F, Giono LE, Fededa JP & de la Mata M (2018) Target RNAs Strike Back on MicroRNAs. *Front Genet* 9

Gascón S, Paez-Gomez JA, Díaz-Guerra M, Scheiffele P & Scholl FG (2008) Dual-promoter lentiviral vectors for constitutive and regulated gene expression in neurons. *J Neurosci Methods*

Gasparini S, Licursi V, Presutti C & Mannironi C (2020) The Secret Garden of Neuronal circRNAs. *Cells* 9: 1815

Ghini F, Rubolino C, Climent M, Simeone I, Marzi MJ & Nicassio F (2018) Endogenous transcripts control miRNA levels and activity in mammalian cells by target-directed miRNA degradation. *Nat*

690 *Commun* 9: 3119

691 Gibson DG, Young L, Chuang R-Y, Venter JC, Hutchison CA & Smith HO (2009) Enzymatic assembly of
692 DNA molecules up to several hundred kilobases. *Nat Methods* 6: 343–345

693 Giusti SA, Vogl AM, Brockmann MM, Vercelli CA, Rein ML, Trumbach D, Wurst W, Cazalla D, Stein V,
694 Deussing JM, *et al* (2014) MicroRNA-9 controls dendritic development by targeting REST. *Elife* 3

695 Guarnerio J, Zhang Y, Cheloni G, Panella R, Mae Katon J, Simpson M, Matsumoto A, Papa A, Loretelli C,
696 Petri A, *et al* (2019) Intragenic antagonistic roles of protein and circRNA in tumorigenesis. *Cell Res*
697 29: 628–640

698 Han J, Han J, Lavigne CA, Jones BT, Zhang H, Gillett F & Mendell JT (2020) A ubiquitin ligase mediates
699 target-directed microRNA decay independently of tailing and trimming. *Science (80-)* 9546: 1–17

700 Hanan M, Simchovitz A, Yayon N, Vaknine S, Cohen-Fultheim R, Karmon M, Madrer N, Rohrlich TM,
701 Maman M, Bennett ER, *et al* (2020) A Parkinson's disease CircRNAs Resource reveals a link between
702 circSLC8A1 and oxidative stress. *EMBO Mol Med*: e11942

703 Hansen TB, Jensen TI, Clausen BH, Bramsen JB, Finsen B, Damgaard CK & Kjems J (2013) Natural RNA
704 circles function as efficient microRNA sponges. *Nature* 495: 384–388

705 Hansen TB, Wiklund ED, Bramsen JB, Villadsen SB, Statham AL, Clark SJ & Kjems J (2011) miRNA-
706 dependent gene silencing involving Ago2-mediated cleavage of a circular antisense RNA. *EMBO J*
707 30: 4414–4422

708 Jeck WR, Sorrentino JA, Wang K, Slevin MK, Burd CE, Liu J, Marzluff WF & Sharpless NE (2013) Circular
709 RNAs are abundant, conserved, and associated with ALU repeats. *RNA* 19: 141–157

710 Jens M & Rajewsky N (2015) Competition between target sites of regulators shapes post-transcriptional
711 gene regulation. *Nat Rev Genet* 16: 113–126

712 Jonas S & Izaurralde E (2015) Towards a molecular understanding of microRNA-mediated gene
713 silencing. *Nat Rev Genet* 16: 421–433

714 Kleaveland B, Shi CY, Stefano J & Bartel DP (2018) A Network of Noncoding Regulatory RNAs Acts in the
715 Mammalian Brain. *Cell* 174: 350-362.e17

716 Kozomara A, Birgaoanu M & Griffiths-Jones S (2019) miRBase: from microRNA sequences to function.
717 *Nucleic Acids Res* 47: D155–D162

718 Kramer MC, Liang D, Tatomer DC, Gold B, March ZM, Cherry S & Wilusz JE (2015) Combinatorial control

719 of Drosophila circular RNA expression by intronic repeats, hnRNPs, and SR proteins. *Genes Dev* 29:
720 2168–2182
721 Kristensen LS, Andersen MS, Stagsted LVW, Ebbesen KK, Hansen TB & Kjems J (2019) The biogenesis,
722 biology and characterization of circular RNAs. *Nat Rev Genet* 20: 675–691
723 Krol J, Busskamp V, Markiewicz I, Stadler MB, Ribi S, Richter J, Duebel J, Bicker S, Fehling HJJ, Schubeler
724 D, *et al* (2010) Characterizing light-regulated retinal microRNAs reveals rapid turnover as a
725 common property of neuronal microRNAs. *Cell* 141: 618–631
726 Lee S, Song J, Kim S, Kim J, Hong Y, Kim Y & Kim D (2013) Selective Degradation of Host MicroRNAs by
727 an Intergenic HCMV Noncoding RNA Accelerates Virus Production. *Cell Host Microbe* 13: 678–690
728 Li JH, Liu S, Zhou H, Qu LH & Yang JH (2014) StarBase v2.0: Decoding miRNA-ceRNA, miRNA-ncRNA and
729 protein-RNA interaction networks from large-scale CLIP-Seq data. *Nucleic Acids Res*
730 Li L, Sheng P, Li T, Fields CJ, Hiers NM, Wang Y, Li J, Guardia CM, Licht JD & Xie M (2021) Widespread
731 microRNA degradation elements in target mRNAs can assist the encoded proteins. *Genes Dev* 35
732 Li X, Liu CX, Xue W, Zhang Y, Jiang S, Yin QF, Wei J, Yao RW, Yang L & Chen LL (2017) Coordinated circRNA
733 Biogenesis and Function with NF90/NF110 in Viral Infection. *Mol Cell* 67: 214-227.e7
734 Liang D & Wilusz JE (2014) Short intronic repeat sequences facilitate circular RNA production. *Genes Dev*
735 28: 2233–2247
736 Liao Y, Smyth GK & Shi W (2014) featureCounts: an efficient general purpose program for assigning
737 sequence reads to genomic features. *Bioinformatics* 30: 923–930
738 Litke JL & Jaffrey SR (2019) Highly efficient expression of circular RNA aptamers in cells using
739 autocatalytic transcripts. *Nat Biotechnol* 37: 667–675
740 Liu CX, Li X, Nan F, Jiang S, Gao X, Guo SK, Xue W, Cui Y, Dong K, Ding H, *et al* (2019) Structure and
741 Degradation of Circular RNAs Regulate PKR Activation in Innate Immunity. *Cell* 177: 865-880.e21
742 Love MI, Huber W & Anders S (2014) Moderated estimation of fold change and dispersion for RNA-seq
743 data with DESeq2. *Genome Biol*
744 Marcinowski L, Tanguy M, Krmpotic A, Rädle B, Lisnić VJ, Tuddenham L, Chane-Woon-Ming B, Ruzsics Z,
745 Erhard F, Benkartek C, *et al* (2012) Degradation of cellular miR-27 by a novel, highly abundant viral
746 transcript is important for efficient virus replication in vivo. *PLoS Pathog* 8
747 Memczak S, Jens M, Elefsinioti A, Torti F, Krueger J, Rybak A, Maier L, Mackowiak SD, Gregersen LH,

748 Munschauer M, *et al* (2013) Circular RNAs are a large class of animal RNAs with regulatory potency.
749 *Nature* 495: 333–338

750 Pamudurti NR, Bartok O, Jens M, Ashwal-Fluss R, Stottmeister C, Ruhe L, Hanan M, Wyler E, Perez-
751 Hernandez D, Ramberger E, *et al* (2017) Translation of CircRNAs. *Mol Cell* 66: 9-21.e7

752 Pawlica P, Moss WN & Steitz JA (2016) Host miRNA degradation by Herpesvirus saimiri small nuclear
753 RNA requires an unstructured interacting region. *RNA* 22: 1181–1189

754 Petkovic S, Graff S, Feller N, Berghaus J, Ruppert V-P, Dülfer J & Sczakiel G (2021) Circular versus linear
755 RNA topology: different modes of RNA-RNA interactions in vitro and in human cells. *RNA Biol*: 1–
756 10

757 Pinzon N, Li B, Martinez L, Sergeeva A, Presumey J, Apparailly F & Seitz H (2017) microRNA target
758 prediction programs predict many false positives. *Genome Res* 27: 234–245

759 Piwecka M, Glažar P, Hernandez-Miranda LR, Memczak S, Wolf SA, Rybak-Wolf A, Filipchyk A, Klironomos
760 F, Cerda Jara CA, Fenske P, *et al* (2017) Loss of a mammalian circular RNA locus causes miRNA
761 deregulation and affects brain function. *Science (80-)* 8526: eaam8526

762 Roditi I, Carrington M & Turner M (1987) Expression of a polypeptide containing a dipeptide repeat is
763 confined to the insect stage of Trypanosoma brucei. *Nature* 325: 272–274

764 Rybak-Wolf A, Stottmeister C, Glažar P, Jens M, Pino N, Hanan M, Behm M, Bartok O, Ashwal-Fluss R,
765 Herzog M, *et al* (2015) Circular RNAs in the Mammalian Brain Are Highly Abundant, Conserved,
766 and Dynamically Expressed. *Mol Cell* 58: 870–885

767 Salzman J, Chen RE, Olsen MN, Wang PL & Brown PO (2013) Cell-type specific features of circular RNA
768 expression. *PLoS Genet* 9: e1003777

769 Sanjana NE, Shalem O & Zhang F (2014) Improved vectors and genome-wide libraries for CRISPR
770 screening. *Nat Methods* doi:10.1038/nmeth.3047 [PREPRINT]

771 Shalem O, Sanjana NE, Hartenian E, Shi X, Scott DA, Mikkelsen TS, Heckl D, Ebert BL, Root DE, Doench
772 JG, *et al* (2014) Genome-scale CRISPR-Cas9 knockout screening in human cells. *Science (80-)*

773 Shi CY, Kingston ER, Kleaveland B, Lin DH, Stubna MW & Bartel DP (2020) The ZSWIM8 ubiquitin ligase
774 mediates target-directed microRNA degradation. *Science (80-)* 370: eabc9359

775 Simeone I, Rubolino C, Noviello TMR, Farinello D, Cerulo L, Marzi MJ & Nicassio F (2022) Prediction and
776 pan-cancer analysis of mammalian transcripts involved in target directed miRNA degradation.

Nucleic Acids Res 50: 2019–2035

Tay Y, Rinn J & Pandolfi PP (2014) The multilayered complexity of ceRNA crosstalk and competition. *Nature* 505: 344–352

Vogl AM, Brockmann MM, Giusti SA, Maccarrone G, Vercelli CA, Bauder CA, Richter JS, Roselli F, Hafner AS, Dedic N, *et al* (2015) Neddylation inhibition impairs spine development, destabilizes synapses and deteriorates cognition. *Nat Neurosci* 18: 239–251

Wickham H (2016) ggplot2: Elegant Graphics for Data Analysis Springer-Verlag New York

Wickham H, Averick M, Bryan J, Chang W, McGowan L, François R, Grolemund G, Hayes A, Henry L, Hester J, *et al* (2019) Welcome to the Tidyverse. *J Open Source Softw*

Xiao MS, Ai Y & Wilusz JE (2020) Biogenesis and Functions of Circular RNAs Come into Focus. *Trends Cell Biol* doi:10.1016/j.tcb.2019.12.004 [PREPRINT]

Yang JH, Li JH, Shao P, Zhou H, Chen YQ & Qu LH (2011) StarBase: A database for exploring microRNA-mRNA interaction maps from Argonaute CLIP-Seq and Degradome-Seq data. *Nucleic Acids Res*

You X, Vlatkovic I, Babic A, Will T, Epstein I, Tushev G, Akbalik GGG, Wang M, Glock C, Quedenau C, *et al* (2015) Neural circular RNAs are derived from synaptic genes and regulated by development and plasticity. *Nat Neurosci* 18: 603–610

Zhang XO, Wang H Bin, Zhang Y, Lu X, Chen LL & Yang L (2014) Complementary sequence-mediated exon circularization. *Cell* 159: 134–147

Zhang Y, Xue W, Li X, Zhang J, Chen S, Zhang JL, Yang L & Chen LL (2016) The Biogenesis of Nascent Circular RNAs. *Cell Rep* 15: 611–624

Figure legends

Figure 1.

System to artificially express circRNAs free of their overlapping, cognate linear RNA.

(A) Top: Illustration of the linear RNA expressing construct used as a positive control for TDMD Bottom: Illustration of the circRNA expressing construct. Depicted with coloured arrows are the sets of primers used to measure the different transcript variants (circular [1], Total Output-TO [2] and linear [3]).

(B) Total output, Linear and circular RNA levels upon expression of the artificial circRNA constructs from the tetracycline-inducible promoter (TREp) bearing perfectly matched or seed-mutant miR-124 sites for selective linear RNA degradation (see Figure S1A).

(C) Total output (left) and circRNA levels (right) upon expression of the artificial circRNA construct versus the linear RNA construct (TDMD inducer). The constructs were expressed from the tetracycline-inducible promoter (TREp) and the synapsin (Syn) promoter respectively in order to achieve similar Total output levels for both constructs. Error bars represent the standard error of the mean (SEM). Statistical significance was determined by unpaired *t* tests (ns: $p > 0.05$, *: $p <= 0.05$, **: $p <= 0.01$, ***: $p <= 0.001$, ****: $p <= 0.0001$).

Figure 2.

Artificial circRNAs are unable to trigger TDMD.

(A) MiR-132 levels upon expression of linear (left) or circular (right) RNAs carrying bulged (TDMD-competent) or seed-mutant miR-132 sites.

(B) AGO2-Flag immunoprecipitation (RIP) followed by RT-qPCR in HEK293T cells. MiR-27a was used to normalize expression (RT-qPCR/Taqman assay). CircRNA expression was measured using circRNA-backspliced-junction specific divergent primers and normalized to miR-27a levels (RT-qPCR/Taqman assay) as an unrelated RISC-loaded miRNA not expected to be affected by the circRNA. Non-specific U6 background binding to Ago2 is shown. As an IP quality control, FLAG/HA-AGO2 input levels were shown to be similar across conditions and efficiently pulled-down using anti-FLAG beads (Figure S2A). Accordingly, miR-27, but not U6 RNA, was efficiently co-immunoprecipitated (Figure S2B).

(C) Subcellular fractionation showing total vs. cytoplasmic (left) and total vs. nuclear (right) fractions, followed by RT-qPCR of the circRNA and linear RNA isoforms, normalized by Gapdh (for cytoplasm) or U6 (for nucleus). Fractionation efficiency was assessed via Western Blot and RT-qPCR (Figure S2C-D). Error bars represent the standard error of the mean (SEM). Statistical significance was determined by unpaired *t* tests (ns: p > 0.05, *: p <= 0.05, **: p <= 0.01, ***: p <= 0.001, ****: p <= 0.0001).

Figure 3.

Endogenous CDR1as/ciRS-7 lacks TDMD activity on miR-7.

(A) Left: CDR1as/ciRS-7 total output (linear plus circular) levels measured by RT-qPCR upon coinfection of either a scrambled shRNA or shCDR1as alone or shCDR1as rescued with a linear version of linCDR1as lacking the shCDR1as site, in mouse cortex primary neurons. Right: MiR-7 levels measured by Taqman RT-qPCR upon coinfection of either a scrambled shRNA or shCDR1as alone or shCDR1as rescued with a linear version of linCDR1as lacking the shCDR1as site, in mouse cortex primary neurons.

(B) Left: CDR1as/ciRS-7 total output levels upon over-expression of linear CDR1as/ciRS-7 (linCDR1as), measured by RT-qPCR, in hippocampal primary neurons. Right: Circular CDR1as/ciRS-7 level upon over-expression of linear CDR1as/ciRS-7, measured by RT-qPCR, in hippocampal primary neurons.

(C) MiR-7 targets levels upon over-expression of linear CDR1as/ciRS-7 measured by RT-qPCR, in hippocampal primary neurons.

(D-E) Re-analyzed data from Piwecka et al. 2017 (Piwecka *et al*, 2017). Shown are mRNA fold changes in cortex neurons of CDR1as/ciRS-7 KO vs. WT mice.

(D) Volcano plot of genes predicted as not targeted by miR-7 are depicted in grey and miR-7 predicted targets in red (p-Adj > 0.05) or blue (p-Adj < 0.05).

(E) Box plot displaying an overall upregulation of predicted miR-7 targets upon CDR1as/ciRS-7 KO.

Error bars represent the standard error of the mean (SEM). Statistical significance was determined by unpaired *t* tests (ns: p > 0.05, *: p <= 0.05, **: p <= 0.01, ***: p <= 0.001, ****: p <= 0.0001).

Figure 4.

CircRNAs potentially stabilize dozens of microRNAs along neuron-like differentiation.

(A) miRNA expression fold changes across differentiation. Plotted are fold changes (log2) in miRNA levels across differentiation versus the expression (RPM) pre-differentiation, coloured by the amount of 'effective' sites in circRNAs.

(B-C) The predicted most highly 'sponged' miRNAs show the highest fold changes across differentiation. Plotted are fold changes (log2) in miRNA levels versus their 'sponging' coefficient score (log10) coloured by quartiles in scatter plot (B) or as a boxplot. Unpaired t-tests are shown between the most sponged and the remaining groups (ns: $p > 0.05$, *: $p <= 0.05$, **: $p <= 0.01$, ***: $p <= 0.001$, ****: $p <= 0.0001$).

(D) Transcription rates does not account for the larger fold change across differentiation observed for the most highly 'sponged' miRNAs. Pri-miRNA levels were taken as a proxy for transcription rates. Scatterplots faceted by 'sponging' coefficient quartiles. Plotted are the fold change (log2) of the miRNAs versus the pri-miR fold change (log2).

(E) circRNA expression fold changes across differentiation. Plotted are the fold changes (log2) in circRNA levels versus the expression (junction reads) pre-differentiation, coloured by the number of 'effective' sites each circRNA has for all miRNAs.

(F) Increasing number of predicted miRNA binding sites does not affect circRNAs levels. Boxplot show the fold change (log2) across differentiation of circRNAs with increasing miRNA sites.

Figure S1.

Artificial circRNA constructs and quality controls.

(A) Table summarizing the constructs generated.

(B) circRNAs are resistant to RNase R digestion, confirming the circular topology of the artificial circRNA. RNase R treated samples from Primary Neurons or HEK293T cells were analyzed by RT-qPCR using divergent primers (primers 1 of Fig. 1) amplifying across the backspliced junction to measure levels of artificial circRNA or regular convergent primers (primers 2 and 3 in Fig 1) to measure levels of total reporter output and cognate linear RNA, respectively.

(C) Top: Agarose gel showing triplicates of the qPCR amplicons obtained with divergent primers against the backsplicing junction of the artificial circRNA, after retro-transcription with two different reverse transcriptases (MMLV-RT & Superscript II) to rule out artifacts due to template switching during cDNA synthesis. Bottom: Sanger sequencing of the amplicons shown above confirming backsplicing junction in HEK293 cells.

(D) Northern blot analysis of RNase R treated or untreated samples from HEK293T cells expressing the indicated artificial circRNA constructs. All constructs were expressed from the tetracycline-inducible promoter (TREp). The asterisk (*) marks a putative mechanically linearized product of the corresponding circRNA.

(E) Quantification by different methods of the linear and circular isoforms from RNase R untreated samples of HEK293T cells (naturally lacking miR132) expressing the indicated constructs. Top panels: digital densitometry quantification of Northern blot bands by ImageJ. Bottom panels: RT-qPCR quantification using primers specific for the circular isoform or for both the linear and circular isoforms combined (Total Output) depicted in Figure 1A. Note that HEK293T cells are devoid of miR132.

Figure S2.

HA-FLAG/AGO2 RIP and cellular fractionation quality controls.

(A) Anti HA Western Blot in non-transfected cells or cells transfected with the artificial circRNA bearing bulged (WT) or seed-mutant (mut) miR-132 sites.

(B) U6 and miR-27 levels were measured to corroborate the efficiency of HA-FLAG/AGO2 immunoprecipitation. Error bars represent the standard error of the mean (SEM). Statistical significance was determined by unpaired *t* tests (ns: $p > 0.05$, *: $p <= 0.05$, **: $p <= 0.01$, ***: $p <= 0.001$, ****: $p <= 0.0001$).

(C) Western Blot showing cells transfected with either the artificial circRNA or the linear control RNA, following subcellular fractionation. α-Tubulin and Histone-3 were used as cytoplasm and nucleus markers, respectively.

(D) GAPDH/U6 ratio measured by RT-qPCR confirmed proper of subcellular fractionation of samples either transfected with the artificial circRNA or the linear control. Statistical significance was

915 determined by a paired *t* test (ns: p > 0.05, *: p <= 0.05, **: p <= 0.01, ***: p <= 0.001, ****: p <=
916 0.0001).
917
918 **Figure S3.**
919 (A) Five examples of potential TDMD-competent binding sites for miR-7 present in CDR1as/ciRS-7.
920 (B) Endogenous circular CDR1as/ciRS-7 normalized levels upon over-expression of the linear version
921 of CDR1as/ciRS-7.
922 (C) Illustration of sgRNAs designed to edit CDR1as/ciRS-7 splicing cites by CRISPR/Cas9.
923 (D-E) CDR1as/ciRS-7 (D) and miR-7 (E) fold changes measured by RT-qPCR upon CRISPR/Cas9 editing
924 of CDR1as/ciRS-7 splicing site in mouse primary neurons.
925 (F) Illustration of the primer pair designs for measuring the different CDR1as/ciRS-7 isoforms
926 (detailed in Materials and Methods).
927 (G-H) Re-analyzed data from (Chen *et al*, 2019). Shown are mRNA fold changes in circCSNK1G3 KD vs.
928 WT PC-3 prostate cancer cell line. (G) Volcano plot of genes predicted as not targeted by miR-
929 181b/d are depicted in grey and miR-181b/d predicted targets in red (p-Adj > 0.05) or blue (p-
930 Adj < 0.05). (H) Box plot displaying an overall upregulation of predicted miR-181b/d targets upon
931 circCSNK1G3 KD.
932 Error bars represent the standard error of the mean (SEM). Statistical significance was determined by
933 unpaired *t* tests (ns: p > 0.05, *: p <= 0.05, **: p <= 0.01, ***: p <= 0.001, ****: p <= 0.0001). For the (D-E)
934 panels, equal variance was assumed.
935
936 **Figure S4.**
937 (A) Network diagram depicting biochemically validated interactions between circRNAs (the seven
938 'most sponging') and the miRNAs they interact with.
939 (B) Model of the protection effect of CDR1as/ciRS-7 on miR-7.

Figure 1

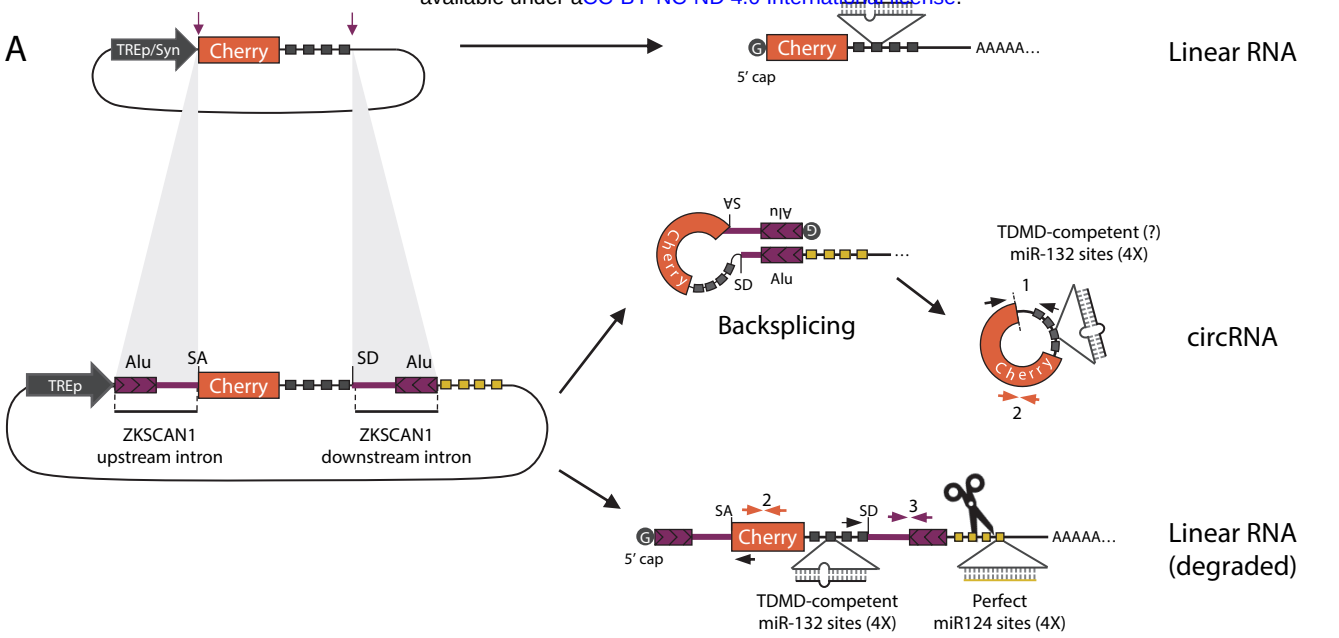

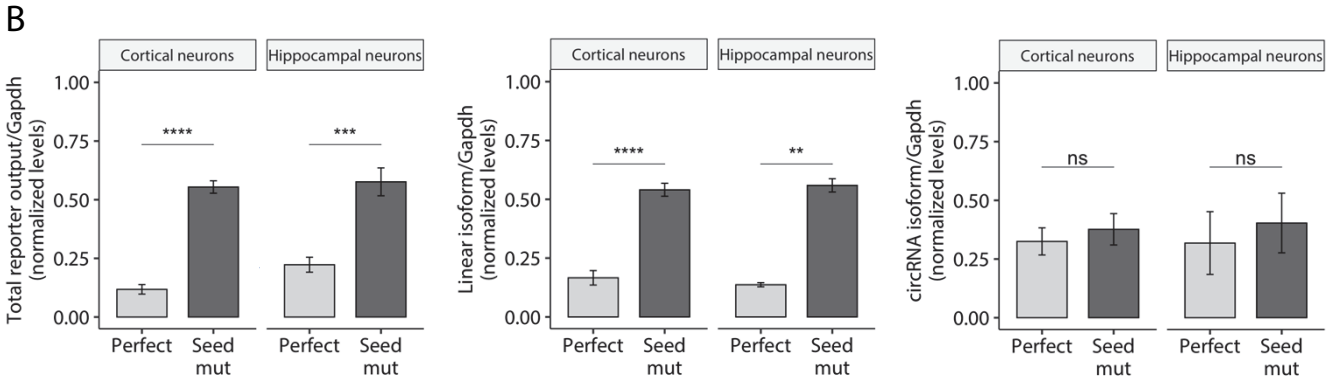

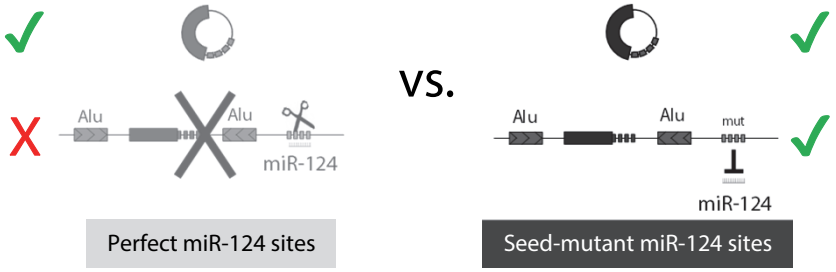

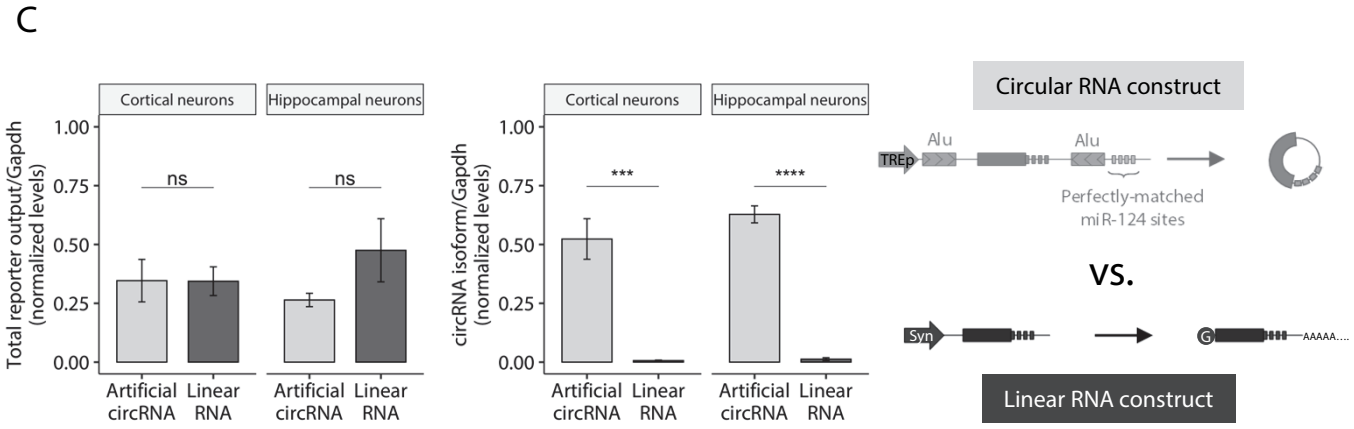

Figure 2

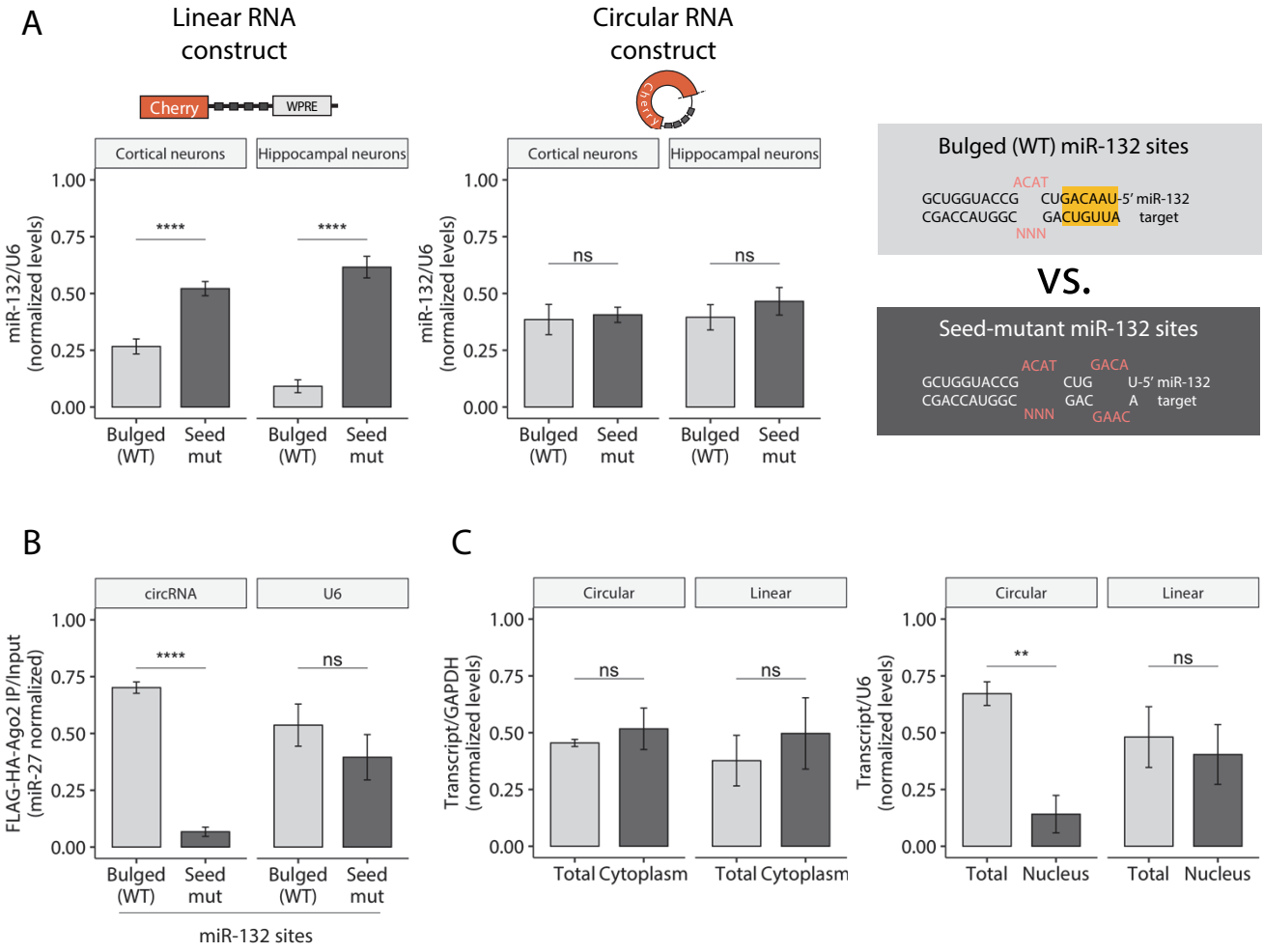

Figure 3

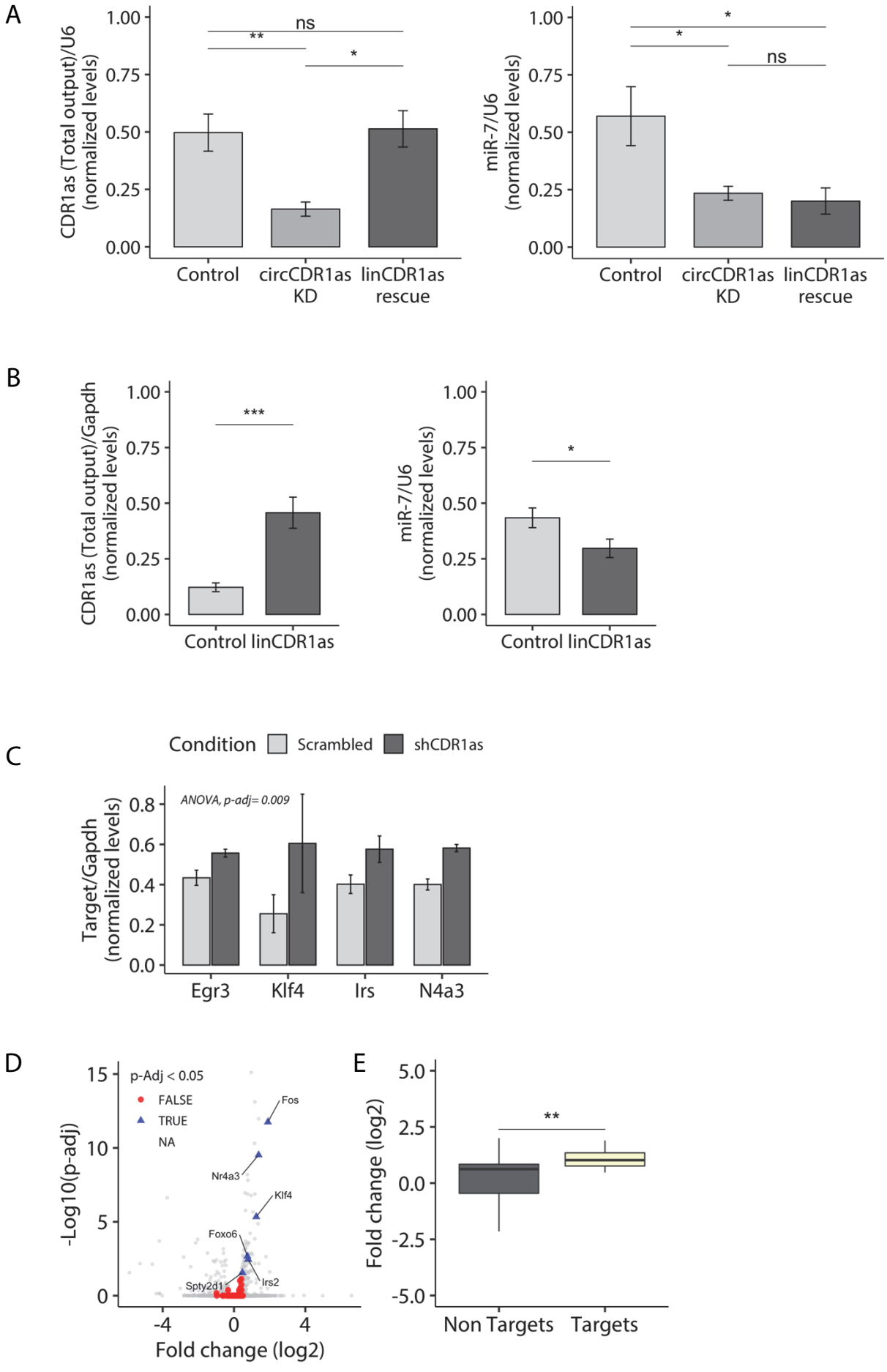

Figure 4

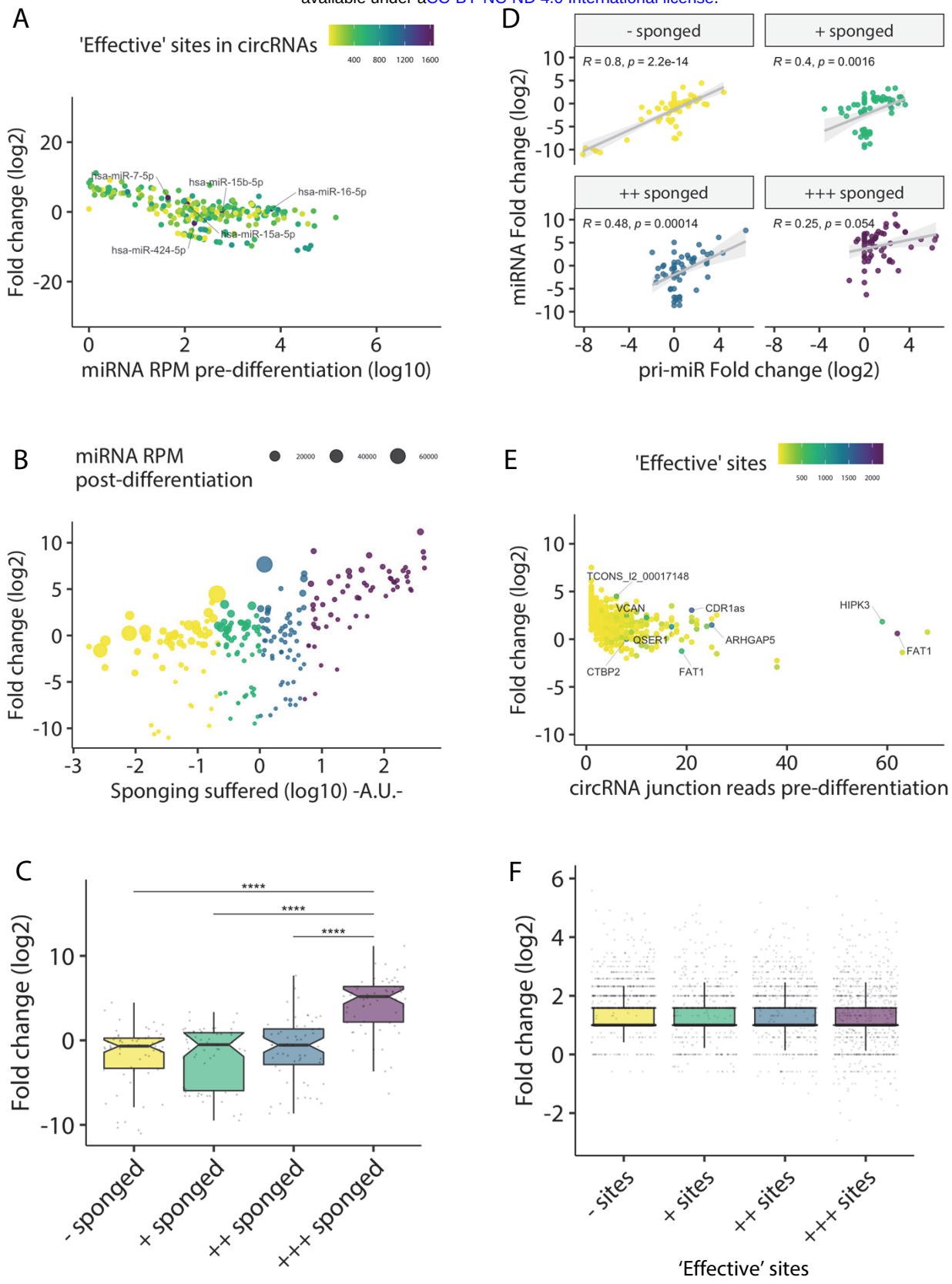

Figure S1

A

Construct purpose	TDMD-inducing sites (miR-132) Type	TDMD-inducing sites (miR-132) Architecture	Linear RNA targeting sites (miR-124) Type	Linear RNA targeting sites (miR-124) Architecture	Expected RNA topology
circRNA expression (linear RNA-depleted)	Bulged (WT)	GCUGGUACCG ACAT CUGACAAU-5′ miR-132 CGACCAUGGC NNN GACUGUUA target	Perfect match	CCGUAAGUGGCGCA CGGAAU-5′ miR-124 GGCAUUCACCGCGU GCCUUA target	Circular
	Seed-mut	GCUGGUACCG ACAT CUG GACA U-5′ miR-132 CGACCAUGGC NNN GAC GAAC A target	Perfect match	CCGUAAGUGGCGCA CGGAAU-5′ miR-124 GGCAUUCACCGCGU GCCUUA target	Circular
circRNA expression (control)	Bulged (WT)	GCUGGUACCG ACAT CUGACAAU-5′ miR-132 CGACCAUGGC NNN GACUGUUA target	Seed-mut	CCGUAAGU GGCG CA CGGA AU-5′ miR-124 GGCAUUCA NNN GU CGGA UA target	Circular + linear leak
	Seed-mut	GCUGGUACCG ACAT CUG GACA U-5′ miR-132 CGACCAUGGC NNN GAC GAAC A target	Seed-mut	CCGUAAGU GGCG CA CGGA AU-5′ miR-124 GGCAUUCA NNN GU CGGA UA target	Circular + linear leak
linear RNA expression (TDMD positive control)	Bulged (WT)	GCUGGUACCG ACAT CUGACAAU-5′ miR-132 CGACCAUGGC NNN GACUGUUA target	NA	NA	Linear
	Seed-mut	GCUGGUACCG ACAT CUG GACA U-5′ miR-132 CGACCAUGGC NNN GAC GAAC A target	NA	NA	Linear

B

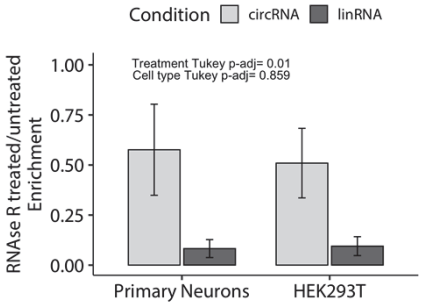

C

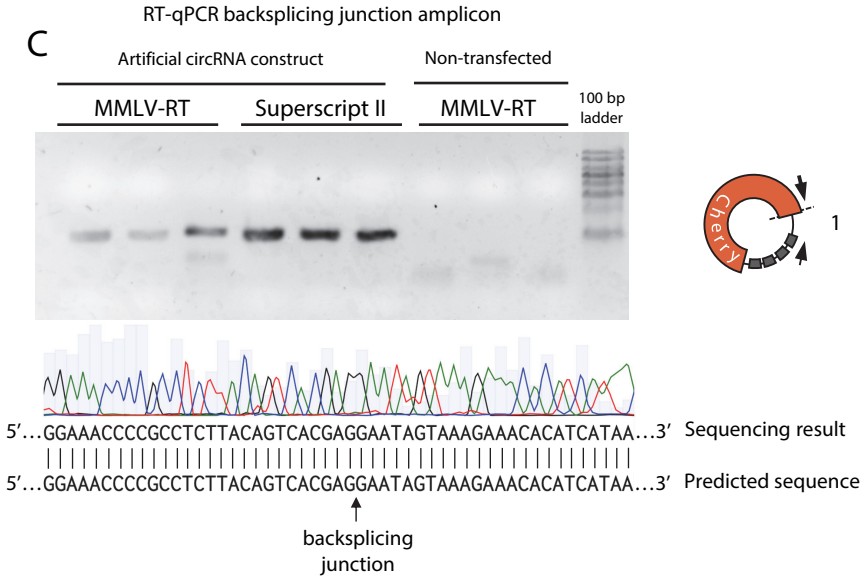

D

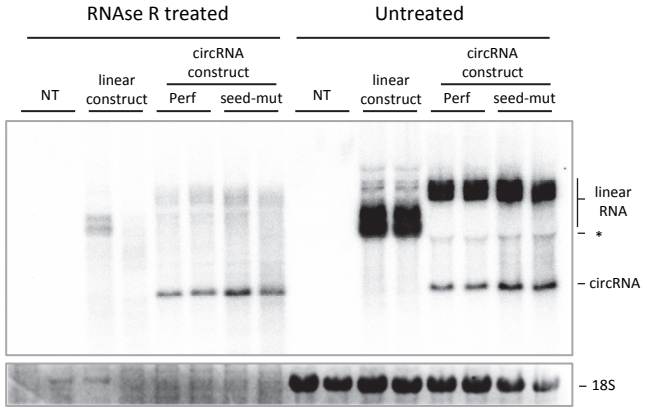

E

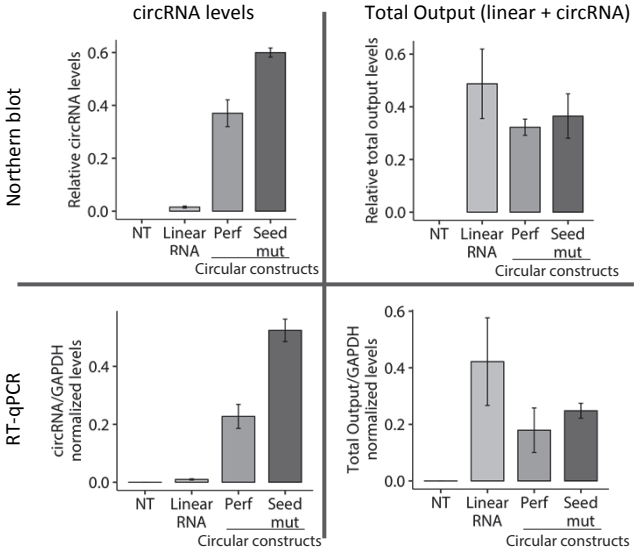

Figure S2

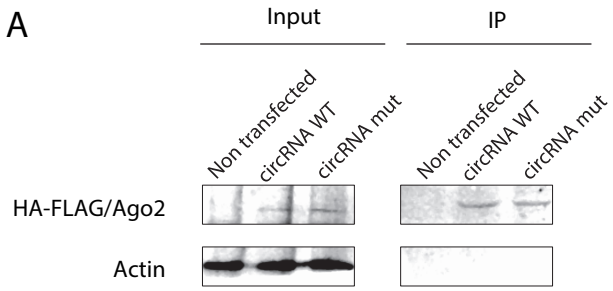

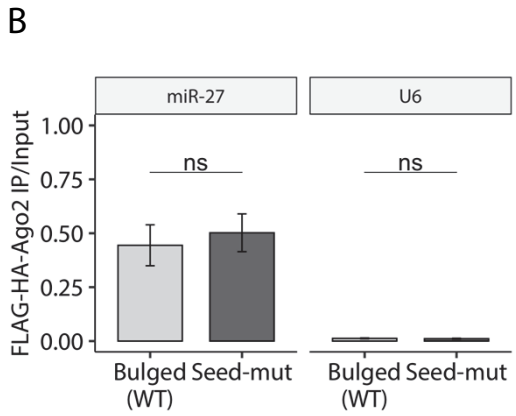

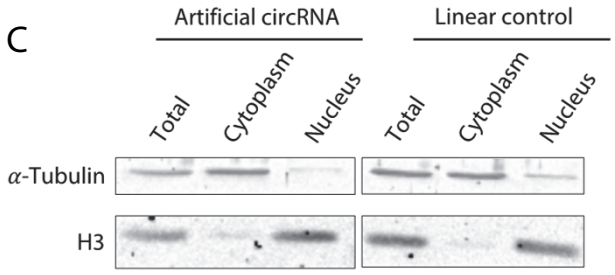

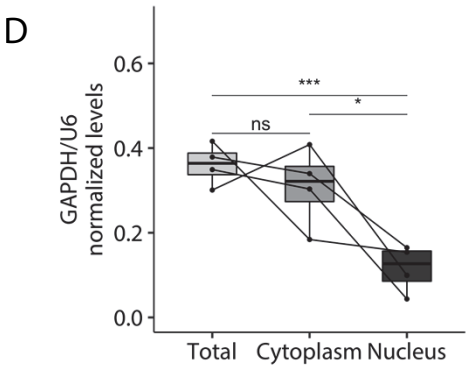

Figure S3

A

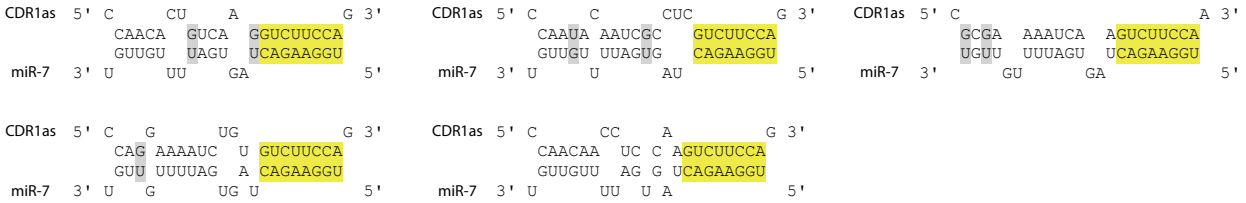

B

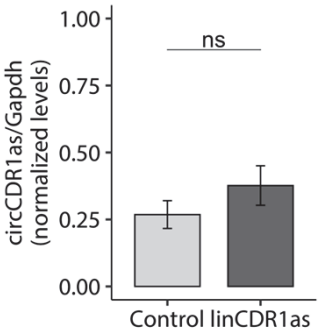

C

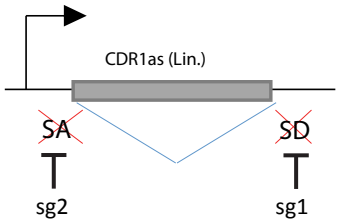

D

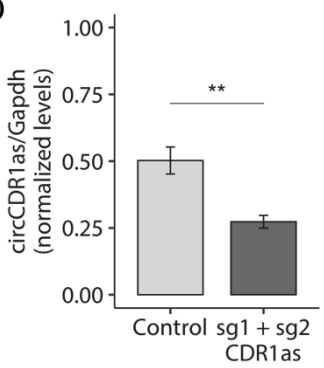

E

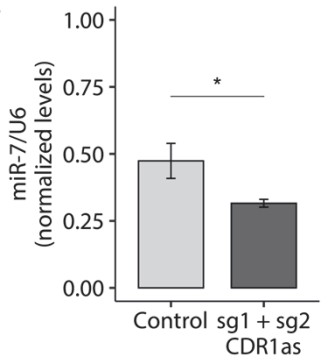

F

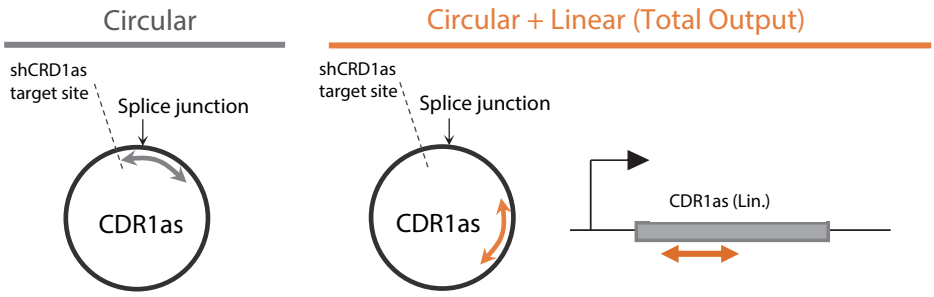

G

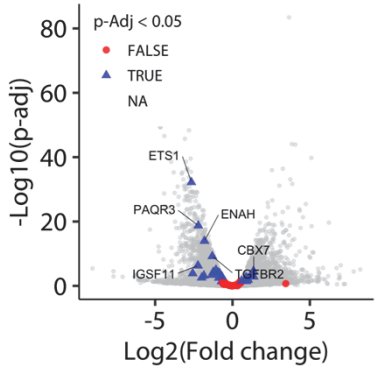

H

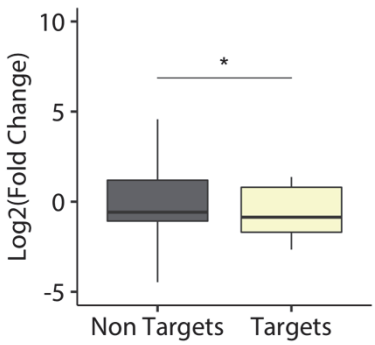

Figure S4

A

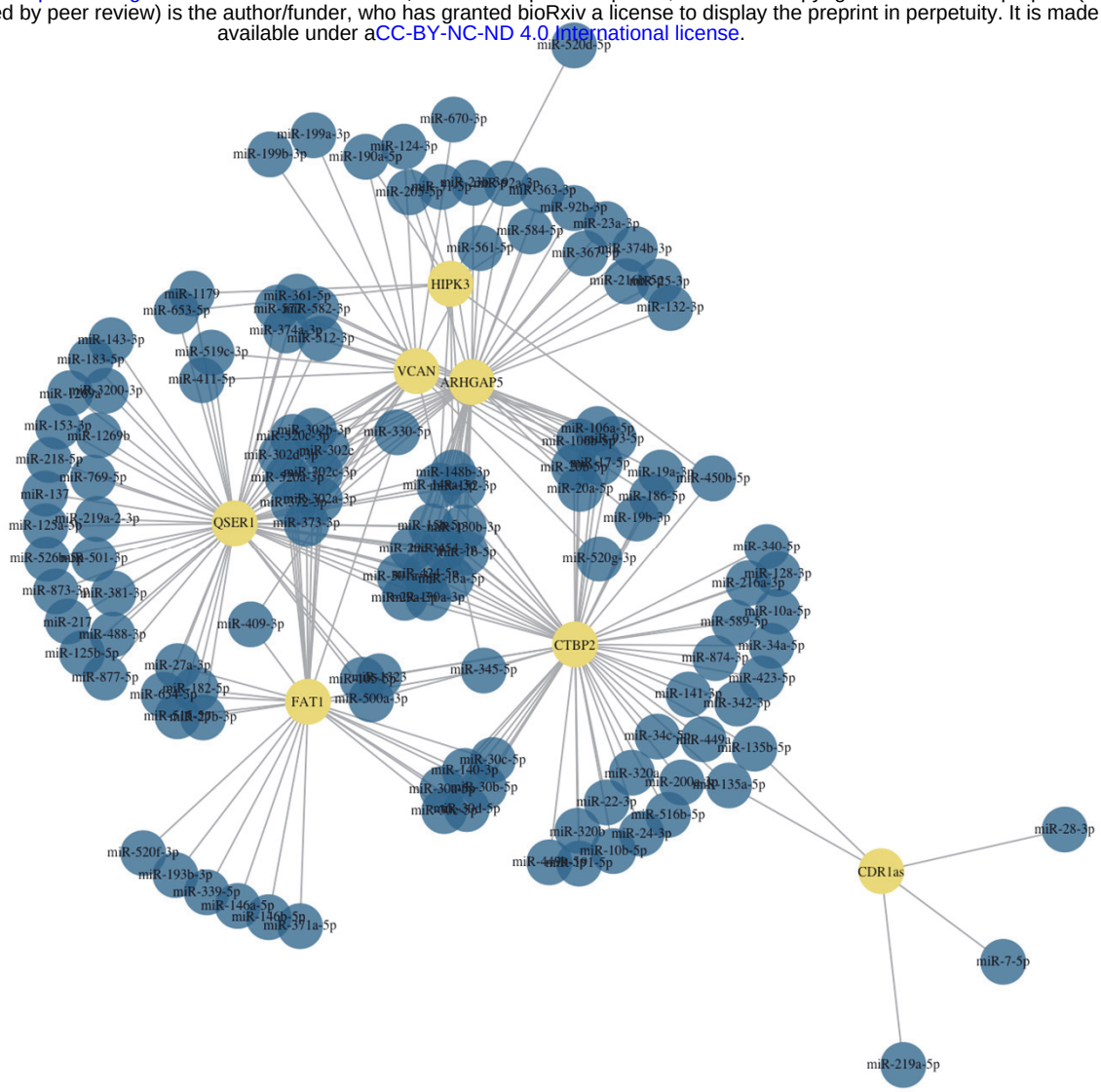

B

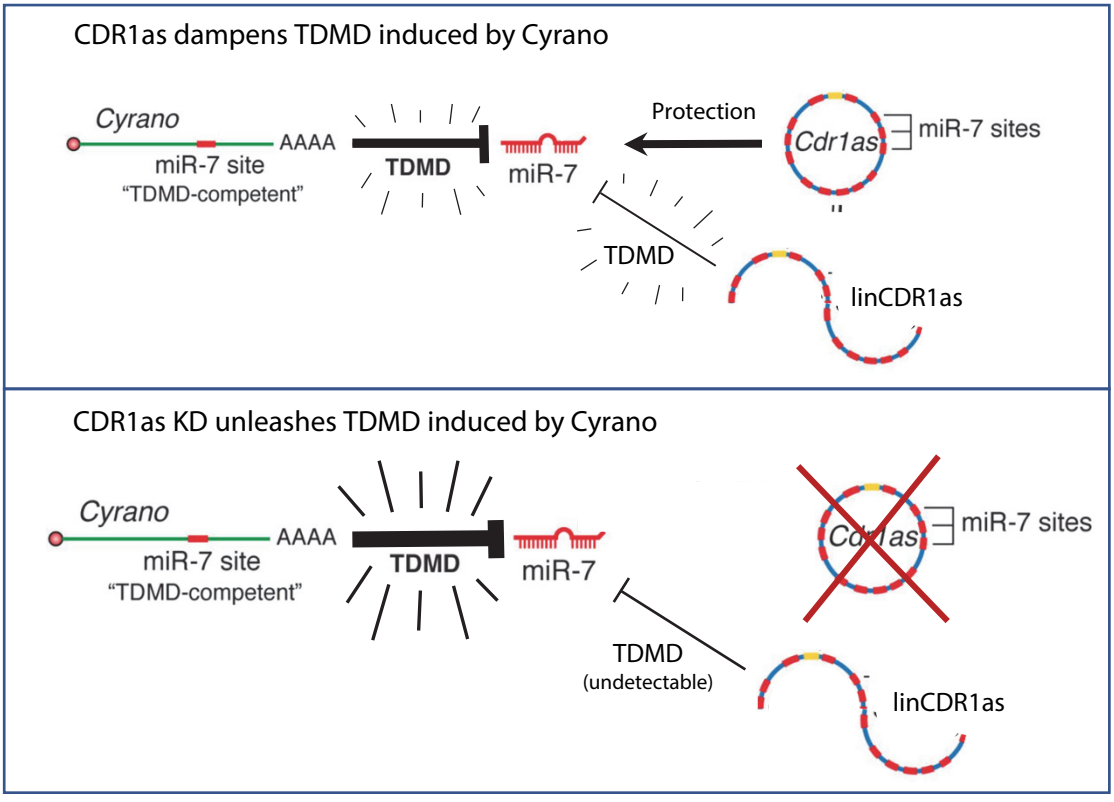

Supplementary Table 1

Oligo name	Use	Sequence 5'->3'
CiRS7_lin_For1	Linear CDR1as	gggtttccagtggtgccagt
CiRS7_lin_Rev1	Linear CDR1as	ctggatacggcagacaccag
ciRS7_lin_For_BamHI	Linear CDR1as lacking miR-671 site	atccGGATCCgggtttccagtggtgccagt
ciRS7_lin_Rev_SalI	Linear CDR1as lacking miR-671 site	atccGTCGACtgaaggaagacacatgtact
rno-miR-671-gblock_mouse-Cir7-match	shCDR1as	atagccgattagttctcgaggatccgggggcagatttgaccggcaggcatc agcagagggctgcttctacaacgctgactacctggcagcccgggcccggc tggctggtgaactggcaggccaggaagaggaggaagccctggagatgct ggaggtgatggatgttttcctccggtgttcagggctccacctctttcgagcc gtagagccagggctggtacagaagttctccctgagggactgcagcccccg gctcagtgaggaactgtaccaccgttgtcgcctcagcaacttggaggggct gctagctcgagcttttggagaatat
miR-7_Bulged_sites	Linear TDMD inducer miR-7 bulged	AGCTGTATAAGTAGGCTAGCCGTCACTGATATGCTCGAAC AACAAAATCTCCGTCTTCCATACAATTTAAAACCCGTCCCA CAACAAAATCACCGTCTTCCATATGCCCGTCCTCTCTCTTTA CAACAAAATCTACGTCTTCCACTTGCAAACCTCACTACAAT ACAACAAAATCGCTGTCTTCCAGTCGACAATCAACCTCTGG A
miR-7_Mut_sites	Linear TDMD inducer miR-7 mutated	AGCTGTATAAGTAGGCTAGCCGTCACTGATATGCTCGAAC AACAAAATCTCCGTACCACATACAATTTAAAACCCGTCCCA CAACAAAATCACCGTACCACATATGCCCGTCCTCTCTCTTT ACAACAAAATCTACGTACCACACTTGCAAACCTCACTACAA TACAACAAAATCGCTGTACCACAGTCGACAATCAACCTCTG GA
SZSCAN1_Ups_intron	Artificial circRNA	gagcgcagtcgagaggatccttttttttttttgacggagtttaacttcttgtctc ccaggtaggaagtgcagtggcgtaatctcggctcactacaacctccacctcc tgggttcaagcgtttctcctgcctcagctttccgagtagctgggattacaggc gcctgccaccatgccctgctgacttttgtatttttagtagagacggggtttcac catgttggccaggctggtcttgaactcctgaccgcaggcgattggcctgcct cggcctcccaaagtgctgagattacaggcgtgagccaccaccccggcctc aggagcgttctgatagtgcctcgatgtgctgcctcctataaagtgttagcag cacagatcacttttttgtaaaggtacgtactaatgacttttttttttatacttcagga atagtaaagaaacacatcataaaacctcccaccggtcgccaccatggtga
SZSCAN1_Downs_intron	Artificial circRNA	taggggaagggaaatgattcaggacgagagtctttgtgctgctgagtgcct gtgatgaagaagcatgttagtgaaaagaattaggctcggcacggtagctca cacctgtaatcccagcactttgggaggctgaggcgggcagatcacttgagg tcaggagtttgagaccagcctggccaacatggtgaaaccttgtctctactaa aaatatgaaaattagccaggcatggtggcacattcctgtaatcccagctactc gggaggctgaggcaggagaatcacttgaacccaggaggtggaggttgca gtaagccgagatcgtaccactgtgctctagccttggtgacagagcgagact gtcttaaaaaaaaaaaagtcgacaatcaacctctgga
pEGFP-miR_BclI_For	pri-miRs	CATCCTGATCATTTTTCGCAACGGGTTTGCC
GFP_Rev	pri-miRs	CTACTTGTACAGCTCGTCCATGC
TREp_XbaI_For	TRE promoter insert	CTACTtctagataggtttaccactccctatc
TREp_BamHI_Rev	TRE promoter insert	CATCCggatccCTAGGCGCGCCTTAATTAAG
sgCiRS7-1_For	sgRNA to mutate CDR1as splice sites	CACCGATGAAACAACTTTCAATACC
sgCiRS7-1_Rev	sgRNA to mutate CDR1as splice sites	AAACGGTATTGAAAGTTGTTTCATC
sgCiRS7-2_For	sgRNA to mutate CDR1as splice sites	CACCGATGATGTTTCCAATATCTAG
sgCiRS7-2_Rev	sgRNA to mutate CDR1as splice sites	AAACCTAGATATTGGAAACATCATC

Supplementary Table 2

Custom-made qPCR Mix	µL per Reaction
*10X Reaction Buffer **	2.5
MgCl2 25 mM	4
Triton x-100 10%	0.06
dNTP mix 10mM	0.5
Glycerol 60%	1.67
DMSO 100%	0.25
Betaine 5M	1.25
*Taq Polymerase (5 U/µL) ***	0.1
*SYBR Green (1/90)****	0.03
Primer Forward 10 µM	0.5
Primers Reverse 10 µM	0.5
H20	8.64
cDNA	5
Final volume	25

* 10X TAS reaction buffer from INBIO Highway

** Taq Polymerase from INBIO Highway

***SYBR Green (Sigma S9430).

***qPCR program:* 94°C-3'; (94°C-15''; 60°C-15''; 72°C-25'') 40x, melting curve. All reactions were run in either an ABI Quantstudio 3 or an ABI StepOnePlus.

Supplementary Table 3

Oligo name	Use	Sequence 5'->3'
CiRS7_For5	Circular CDR1as divergent	cctacaactgcccagtgtctc
CiRS7_Rev2	Circular CDR1as divergent	ggtactggcaccactggaaa
CiRS7_For1	Circular + linear CDR1as (total output)	tgtgtcttccttcacctccag
CiRS7_lin_Rev1	Circular + linear CDR1as (total output)	ctggatacggcagacaccag
qWPRE_For	Linear CDR1as/artificial linRNA control exclusively	actgtgtttgctgacgcaac
qWPRE_Rev	Linear CDR1as/artificial linRNA control exclusively	caacaccacggaattgtcag
miR132 _Artificial_Circ_For	Circular artificial circRNA divergent	TACAAGTAAAGCGGCCGCGTCG
Artificial_Circ_Rev	Circular artificial circRNA divergent	CTCGCCCTTGCTCACCATGGTG
mCherry_seq_For	Circular + linear artificial circRNA (Total output)	gtggaacagtacgaacgcgcc
Linker-2_BsrGI_Rev	Circular + linear artificial circRNA (Total output)	CTACTTGTACATATGATTAGTGGTTTAAA
ZSCAN1_down_Seq_Rev	Linear artificial leak exclusively (combined with Artificial_circ_For)	TGAGCTACCGTGCCGAGCCTAA
Klf4f	miR-7 Target	aaaagaacagccaccacac
Klf4r	miR-7 Target	tcccagtcacagtggtaagg
Egr3f	miR-7 Target	cgcgctcaacctcttctc
Egr3r	miR-7 Target	attgggcttctcgttggtc
Irs2f	miR-7 Target	gagtgtgtgggggtccag
Irs2r	miR-7 Target	aatgtagaattgctcccgttg
Nr4a3f	miR-7 Target	tgcctgtcagcactgagtatg
Nr4a3r	miR-7 Target	agagcctgtcccttcctgt